

NASA Contractor Report 3135

NASA
CR
3135
c.1



TECH LIBRARY KAFB, NM

LOAN COPY: RETURN TO
AFWL TECHNICAL LIBRARY
KIRTLAND AFB, TN, TN

Extended Analytical Study of the Free-Wing/Free-Trimmer Concept

Richard F. Porter, David W. Hall,
and Rodolfo D. Vergara

CONTRACT NAS4-2498
APRIL 1979





NASA Contractor Report 3135

Extended Analytical Study of the Free-Wing/Free-Trimmer Concept

Richard F. Porter, David W. Hall,
and Rodolfo D. Vergara
Battelle Columbus Laboratories
Columbus, Ohio

Prepared for
Dryden Flight Research Center
under Contract NAS4-2498



National Aeronautics
and Space Administration

**Scientific and Technical
Information Office**

1979

TABLE OF CONTENTS

	<u>Page</u>
SUMMARY	1
INTRODUCTION	2
Free-Wing Concept	2
Free-Wing/Free-Trimmer Concept	4
Previous Work	4
Purpose of This Investigation	7
Scope	7
SYMBOLS	8
PROCEDURE	10
Mathematical Models	10
Longitudinal Equations	10
Lateral-Directional Equations	10
Aerodynamic and Mass Parameters	12
Conceptual Aircraft Designs	12
Handling Qualities Criteria	12
Responses to Atmospheric Turbulence	12
DISCUSSION OF RESULTS	14
Forward Trimmer Configurations	14
Results of Previous Study	14
Motivation of Current Study	17
Candidate Configurations	17
Comparison of Forward-Trimmer Configurations	19
Control Response Characteristics	21
Effect of Wing Sweep	24

TABLE OF CONTENTS
(CONTINUED)

	<u>Page</u>
Aft Trimmer Configurations	24
Results of Previous Study	24
Rationale of Current Study	25
Free Aft-Trimmer Capabilities	25
Fixed Aft-Trimmer Capabilities	26
Longitudinal Characteristics of Aft Trimmers	28
Longitudinal Control Responses	28
Longitudinal Effects of Wing Sweep Angle	32
Lateral-Directional Behavior	33
Summary of Configuration Options	42
CONCLUSIONS	44
APPENDIX A. EQUATIONS OF MOTION	46
Introduction	46
Symbols	46
Longitudinal Equations	46
Lateral-Directional Equations.	49
Coordinate Systems	52
Longitudinal Equations	54
Trimmer Angle of Attack	54
Trimmer Lift Coefficient	55
Trimmer Pitching Moment Equation	55
Longitudinal Components of Trimmer Hinge Force	57
Normal Component of Trimmer Hinge Force	57

TABLE OF CONTENTS
(Continued)

	<u>Page</u>
Wing Angle of Attack	58
Wing Lift Coefficient	58
Longitudinal Component of Wing Hinge Force	59
Normal Component of Wing Hinge Force	60
Wing Pitching Moment Equation	60
Fuselage Pitching Moment Equation	61
Airspeed	62
Fuselage Angle of Attack	63
Lateral-Directional Equations	63
Rolling Moment Equation	64
Yawing Moment Equation	64
Side Force Equation	64
Right Trimmer Hinge Moment Equation	64
Lateral Path Displacement Equation	64
APPENDIX B. LINEAR APPROXIMATION OF UNSTEADY AERODYNAMIC EFFECTS	65
APPENDIX C. AERODYNAMIC AND MASS PARAMETERS	68
Symbols	68
Longitudinal Parameters	70
Lift-Curve Slope	70
Mutual Interference Coefficients	71
Drag Coefficients	72
Fuselage-Tail Lift-Curve Slope	72
Fuselage Static Angle of Attack Stability	72

TABLE OF CONTENTS
(Continued)

	<u>Page</u>
Pitch Damping Coefficient	72
Longitudinal Mass Parameters	72
Lateral-Directional Parameters	73
Wing-Trimmer Contributions to Lateral-Directional Derivatives	73
Fuselage/Tail Contributions to Lateral-Directional Derivatives	74
Lateral-Directional Mass Parameters	79
APPENDIX D. METHOD OF COMPUTING TURBULENCE RESPONSES	81
Symbols	81
Longitudinal Responses	81
Lateral-Directional Responses	82
REFERENCES	84

LIST OF TABLES

Table I.	Trimmed C_{LMAX} of Candidate Configurations	19
Table II.	Evaluation Criteria for Forward Trimmer Configuration with Three Wing Sweep Angles	25
Table III.	Longitudinal Criteria for Aft Trimmer Configurations with Three Wing Sweep Angles	32
Table IV.	Lateral-Directional Characteristics Straight Wing/ Free Aft Trimmer	35
Table V.	Lateral-Directional Characteristics Straight Wing/ Fixed Aft Trimmer	36
Table VI.	Lateral-Directional Characteristics Equivalent Conventional Aircraft.	37

TABLE OF CONTENTS
(Continued)

		<u>Page</u>
Table VII.	Lateral-Directional Responses to Unit Turbulence Intensity	40
Table VIII.	Trade-Off Comparison of Configurations.	44
Table IX.	Results of Indicial Response Computations	67
Table X.	Lift Curve Slopes	70
Table XI.	Mutual Interference Coefficients	71
Table XII.	Longitudinal Mass Parameters for Wing/Trimmer Assembly	73
Table XIII.	Wing and Trimmer Contributions to Lateral-Directional Derivatives for Cruise Condition, Straight Wing . . .	75
Table XIV.	Wing and Trimmer Contributions to Lateral-Directional Derivatives for Approach Condition.	76
Table XV.	Fuselage Assembly Contributions to Lateral-Directional Derivatives	80
Table XVI.	Moments and Products of Inertia	80

LIST OF FIGURES

Figure 1.	Cross-Sectional Illustration of the Free Wing	3
Figure 2.	Baseline Light Aircraft with Straight Free Wing and Aft Trimmer	13
Figure 3.	Forward Trimmer Configuration From Reference 8 . . .	15
Figure 4.	Vertical Gust Responses Illustrating Adverse Transient Effect of Forward Trimmer	16
Figure 5.	Free-Trimmer Configurations Yielding the Same Trimmed $C_{L_{MAX}}$	18

LIST OF FIGURES
(Continued)

	<u>Page</u>
Figure 6. Comparison of Candidate Forward Trimmer Configurations	20
Figure 7. Selected Forward Trimmer Configuration	22
Figure 8. Response to Step Longitudinal Control Input, Forward Trimmer/Straight Wing, Cruise.	23
Figure 9. Trim Characteristics, Straight Wing/Aft Fixed Trimmer.	26
Figure 10. Longitudinal Comparison of Free and Fixed Aft Trimmers Straight Wing, Cruise	29
Figure 11. Response to Step Longitudinal Control Input, Free Aft Trimmer/Straight Wing, Cruise.	30
Figure 12. Response to Step Longitudinal Control Input, Fixed Aft Trimmer/Straight Wing, Cruise.	31
Figure 13. Aft Trimmer Configuration with 10° Sweep	34
Figure 14. Lateral Directional Turbulence Responses of Aft Trimmer Configurations, Approach, Zero Fuselage Deck Angle	39
Figure 15. Responses to Step Lateral Control Input, Free Trimmer Configuration.	41
Figure 16. Responses to Step Lateral Control Input, Fixed Trimmer Configuration	43
Figure 17. Illustration of Axis Systems	53

EXTENDED ANALYTICAL STUDY OF THE FREE-WING/FREE-TRIMMER CONCEPT

Richard F. Porter, David W. Hall, and Rodolfo D. Vergara
Battelle Columbus Laboratories

SUMMARY

This report describes an extension of the analytical study of the free-wing/free-trimmer concept which was documented in NASA Contractor Report 2946.

Earlier studies had indicated several benefits, including stall-proof behavior and substantial gust alleviation, for aircraft employing an unconventional wing, free to pivot about a spanwise axis forward of its aerodynamic center and trimmed, independently of the fuselage, by a trailing-edge control tab. A disadvantage of this basic concept is the relatively low wing lift coefficient available, since high-lift trailing-edge flaps are precluded by their associated negative pitching moments.

The free wing/free trimmer is a concept intended to provide sufficient trimming power to permit the use of high-lift trailing-edge flaps on free-wing aircraft. The wing is controlled by the pitching moment produced about its hinge axis by the aerodynamic forces on a smaller, external trimmer surface attached to the wing by a boom or equivalent structure. Furthermore, the trimmer itself is free to pivot about a spanwise axis forward of its aerodynamic center. Pitch control of the entire assembly is maintained by deflection of a trailing-edge tab on the trimmer surface.

The free-wing/free-trimmer concept was analyzed in CR-2946. Both forward (canard) and aft-mounted free trimmers of equal area were considered, but only longitudinal behavior was examined. Despite an inherently greater lift potential, the forward free trimmers were found to have inferior dynamic characteristics when compared to aft free-trimmers; while the aft trimmers incurred a greater weight penalty.

The analytical study described in this report expands the previous work to: (1) compare the fore and aft trimmer configurations on the basis of equal lift capability, rather than equal area; (2) assess the influence of aft trimmers, both free and fixed, on the lateral-directional modes and turbulence

responses; (3) examine the feasibility of using differential deflection of the aft trimmers for lateral control; (4) determine the effects of independent fuselage attitude (deck angle) on lateral-directional behavior; and (5) estimate the influence of wing sweep on dynamic behavior and structural weight.

The aft-mounted trimmers were placed outboard of the wing tips in all cases.

It was concluded that the forward trimmer concept is feasible with the reduced size examined in this study, but that it remains inferior to the aft trimmer arrangement in every respect except structural weight. The aft free-trimmer configuration has excellent vertical gust alleviation and good control response behavior but exhibits an amplified rolling motion in turbulence.

If the aft trimmer is not free to respond to local flow conditions, the weight penalty is reduced and the trimmed lift capability can be increased substantially for the same wing/trimmer geometry. The amplified rolling response to turbulence of the free trimmer is eliminated, but the fixed trimmer suffers some reduction in vertical gust alleviation.

Differential motion of the aft trimmer, either free or fixed, was found to provide powerful and effective lateral control. The effect of fuselage deck angle is largely confined to a reduction of the dutch roll damping ratio for nose-down attitudes.

Wing sweep angle has a minor effect on dynamic characteristics, but some wing sweep is structurally advantageous for the aft trimmer configurations.

INTRODUCTION

Free-Wing Concept

A free wing is an aerodynamic lifting surface which is completely free to rotate about a spanwise axis, subject only to aerodynamic pitching moments and unrestricted by mechanical constraints. To provide static angle of attack stability, the axis of rotation is located forward of the aerodynamic center of the wing panel.

Figure 1 is an illustration of a free-wing configuration in which the equilibrium angle of attack is established through a balance of moments created by a trailing-edge control surface and the torques produced by the lift and drag forces.

The concept of a free wing controlled by a trailing-edge surface was disclosed in a patent, now expired, which was issued in 1944 to Daniel R. Zuck. Zuck built a small prototype aircraft in 1945 as a private venture, but this aircraft was never flown.

An independent development of a different form of the free wing was also begun by George C. Spratt in the early 1940's. Spratt's "Controlwing"

differs from Zuck's concept in that no trailing-edge control surface is used. Instead, the equilibrium angle of attack is pre-set by the location of the hinge axis, slightly forward and below the wing aerodynamic center. In flight, the aircraft is a constant-speed airplane, with rate of climb or descent controlled by engine power. Mr. Spratt has extensive flight experience with a small "Controlwing" flying boat as described in reference 1.

Except for control system responses, the Zuck and Spratt configurations are dynamically similar for symmetric longitudinal motion. In both instances, the wing has complete mechanical pitch freedom to seek and maintain its intended equilibrium lift coefficient independent of the pitch attitude of the fuselage assembly.

The primary motivation of both Zuck and Spratt has been to produce a stall-proof airplane. With suitable mechanical limitation on control surface displacement (Zuck) or hinge axis location (Spratt), the wing cannot be forced into the stall regime. Furthermore, the anti-stall behavior is not influenced by center of gravity variations in the fuselage assembly.

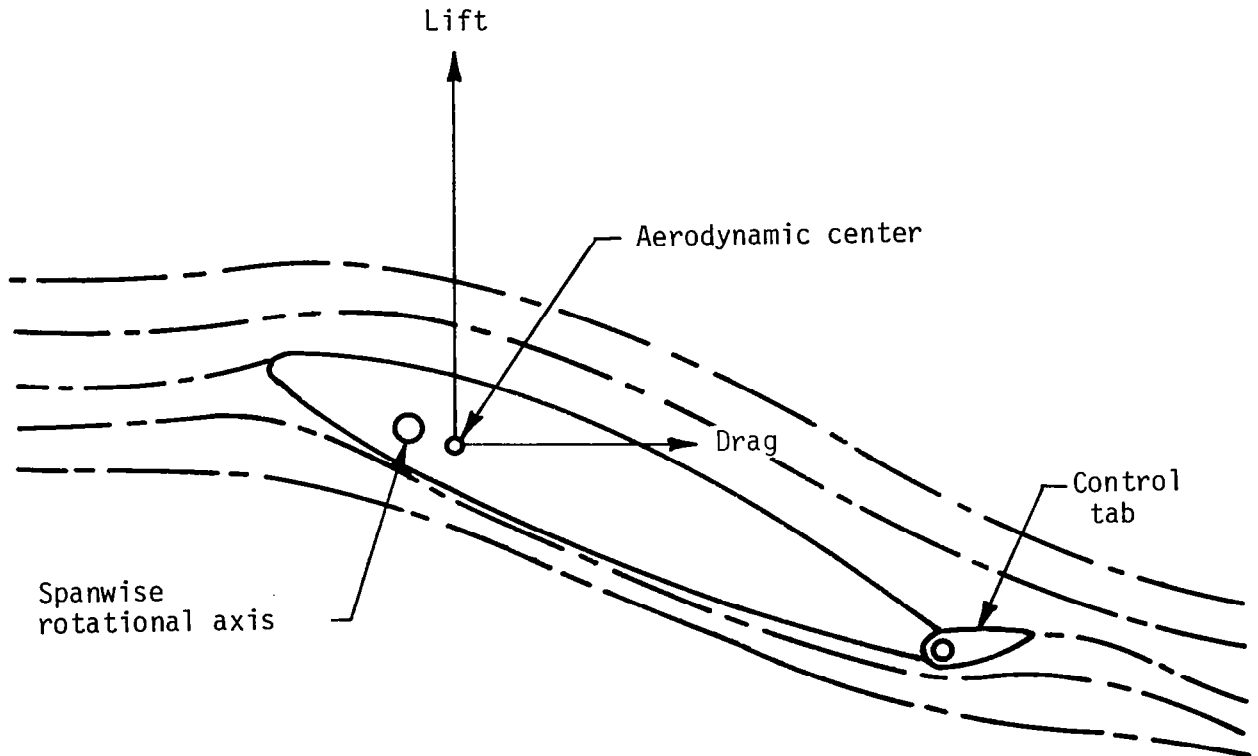


FIGURE 1. CROSS-SECTIONAL ILLUSTRATION OF THE FREE WING

An additional major benefit of the free-wing concept is substantial alleviation of the normal load factor response to vertical gusts. The gust alleviation arises from the tendency of a stable lifting surface to maintain a prescribed lift coefficient by responding to the natural pitching moments which accompany changes in flow direction. While all stable aircraft tend to relieve the lift increment due to a vertical gust by pitching into the relative wind, the rapidity of the alleviating motion depends upon the pitching moment of inertia. Because of the greatly reduced inertia of the wing panel, compared to the aircraft as a whole, the free-wing concept provides a significant reduction in the turbulence response.

A further attribute, which may have certain specialized mission applications, is an inherent fuselage pointing capability by which the fuselage assembly may be trimmed through a wide range of deck angles independent of the pitch attitude of the wing. This feature could be used for weapon or sensor pointing as well as thrust vectoring.

Free-Wing/Free-Trimmer Concept

A disadvantage of the basic free-wing concept is the relatively low maximum lift coefficient. Since there is no mechanism to overcome the powerful negative pitching moments inherent in high-lift trailing-edge flap deflection, lift augmentation is limited to the use of leading-edge slats.

The free-wing/free-trimmer is a NASA conceived extension of the free wing concept intended to provide sufficient trimming power to permit the use of high-lift flaps on free-wing aircraft. The wing is controlled by the pitching moment produced about its hinge axis by the aerodynamic forces on a smaller, external trimmer surface attached to the wing by a boom or equivalent structure. Furthermore, the trimmer itself is a small free-wing surface, free to pivot about a spanwise axis forward of its aerodynamic center. Pitch control of the entire assembly is obtained by deflection of a trailing-edge tab on the free trimming surface.

Previous Work

The first known analytical study to predict the fundamental dynamic behavior of basic free-wing aircraft permitted independent motion of the left and right wing panels and is reported in reference 2. The following conclusions were drawn from this earlier work.

(1) Most atmospheric turbulence effects were greatly reduced, particularly in the root-mean-square (rms) load factor (62 percent reduction) and rolling disturbances (25 percent reduction). On the other hand, the rms fuselage pitch rate was increased about 180 percent in comparison with equivalent fixed-wing aircraft.

(2) All stick-fixed modes of motion were stable except for the spiral mode, where the rate of divergence was found to be excessively high in

the approach condition.

(3) With independent left and right wing panel freedom, the lateral-directional handling qualities were unsatisfactory because of the combination of low roll damping and spiral divergence.

(4) Artificial stability augmentation, in the form of a simple roll damper, provided excellent lateral control and turbulence penetration characteristics.

As a result of the very substantial gust alleviation predicted in reference 2, a second study was performed to provide a realistic and comprehensive assessment of the practical aspects of the implementation of the free-wing concept for light, general aviation aircraft.

The second investigation is reported in reference 3. This study, while analytical, was supported by limited wind-tunnel experiments.

From the results of the second study, the following conclusions were drawn:

(1) The free-wing concept can be applied to unsophisticated low wing loading light aircraft to provide a ride quality, based on normal load factor attenuation, equal or superior to that of aircraft employing much higher wing loadings. Compared to similar light aircraft in cruise flight, reductions of about 54 percent can be realized in the rms load factor increments in continuous turbulence.

(2) For free-wing aircraft without differential wing panel freedom, all pertinent handling qualities and certification criteria can be met without recourse to stability augmentation, either active or passive.

(3) Differential pitch freedom between the left and right wing panels should not be permitted for aircraft in this class, although it appears that passive mechanical devices can be applied to correct the serious lateral deficiencies which accompany such freedom.

(4) Leading-edge slats are necessary for takeoff and landing to compensate for the inherent low maximum trimmed lift coefficients obtained with trailing-edge control surfaces.

(5) The free-wing panels should be balanced about the spanwise hinge axis with leading-edge slats retracted. A ballast weight penalty is incurred which might range from 1.5 percent to 7.0 percent of the aircraft gross weight, depending on the detailed design.

Reference 4 describes an experimental wind tunnel investigation of the static and dynamic stability characteristics of a tilt-propeller free-wing V/STOL aircraft. A major objective of the investigation was to observe the dynamic characteristics of the free wing under stalled trim conditions. A stall flutter phenomenon, consisting of self-sustained oscillations in the

stall region, was observed when sufficiently large trailing-edge tab deflections were used. Reducing the control tab deflection was effective in terminating the oscillations, indicating that control tab deflection limiting would be effective in preventing the stall flutter oscillation. Since the flutter threshold is very near the maximum wing lift coefficient, it was concluded that suitable control deflection limits would not seriously reduce the wing lift capability.

Two pertinent experimental investigations using radio controlled models have been reported. In the first of these, described in references 5 and 6, the free wing was controlled by a pair of separate trailing edge surfaces at the wing tips. In the second, a radio controlled model test program represented the initial exploration of the free-wing/free-trimmer concept and is described in reference 7. The radio controlled airplane model having a free wing with free canard was flown to assess its flight characteristics, controllability, and potential operating problems. The test vehicle was flown through a series of maneuvers designed to permit the evaluation of certain characteristics by observation. Stall/spin characteristics were considered to be excellent, and no effect on longitudinal stability was observed when center of gravity changes were made. Lack of onboard instrumentation precluded any conclusions about gust alleviation.

The analytical study of reference 8 was performed to investigate the longitudinal behavior of representative small free-wing/free-trimmer aircraft. Canard trimmer arrangements, similar to the radio controlled model of reference 7, were examined as well as configurations in which the free trimmers were mounted at the wingtips aft of the wing hinge axis. The study was limited to linear analyses of the responses to symmetric vertical gusts and to the basic longitudinal flying qualities as indicated by the characteristic roots associated with the stick-fixed longitudinal modes.

The following conclusions were reached in reference 8:

(1) For the trimmer area ratio considered (1/6), the most promising configuration employs wingtip-mounted trimming surfaces placed aft of the wing hinge line with a moment arm of one wing chord length. Of the configurations examined, this arrangement alone could provide excellent alleviation of vertical gust loads while (a) exceeding the maximum lift capability of pure free-wing configurations and (b) meeting fundamental criteria for the stability of the stick-fixed longitudinal modes.

(2) For vertical gust alleviation, forward trimmers are inferior to aft-mounted surfaces because of adverse wing pitching moments caused by transient aerodynamic forces on the trimming surfaces.

(3) Mass balancing of the trimmer surface about its hinge axis is vital for precluding adverse effects on the stability of the characteristic modes. In particular, aft imbalance must be avoided.

(4) Longitudinal displacement of the center of gravity of the fuselage assembly appears to be more significant for free-wing/free-trimmer

configurations than for pure free-wing aircraft. Forward displacement decreases the damping of the phugoid mode while aft displacement decreases the damping of one of the short-period modes. The effect of fuselage imbalance is more pronounced for slow-speed flight, and the sensitivity depends upon the aerodynamic design of the fuselage assembly.

(5) Small variations in the wing assembly center of gravity (of the order of a few percent of wing chord) have no significant effect on the inflight characteristic modes, but center of gravity locations aft of the wing hinge axis should be avoided to facilitate smooth landings.

(6) Forward-trimmer configurations are more efficient from a weight standpoint than aft trimmers, and could, if properly sized and placed, provide a lighter total wing weight than a pure free wing. The aft-trimmer configuration incurs a higher weight penalty because of the additional counterweight needed to balance the wing assembly about its hinge axis.

Purpose of This Investigation

The purpose of the current study was to extend the analysis which was begun in reference 8. A general objective was to bring the understanding of free-wing/free-trimmer aircraft dynamics to a level roughly equivalent to that which exists for pure free-wing aircraft (references 2 and 3).

Specific objectives were to:

(1) Extend the analysis to include the lateral-directional behavior of free-wing/free-trimmer aircraft.

(2) Augment the previous longitudinal work with a more in-depth comparison of forward and aft trimmer configurations.

(3) Examine the potential merits of tip-mounted aft trimmers which can be displaced only by pilot action and are not free to respond passively to local airflow changes.

Scope

The research effort described in this report is limited to an analytical study of the characteristic stick-fixed modes and atmosphere turbulence responses of hypothetical small free-wing aircraft with external trimming surfaces. Attention is confined to linear analyses of uncoupled longitudinal and lateral-directional motion.

For forward-mounted (canard) trimmers, only a one-piece, free-trimming surface is considered; furthermore, for these configurations, only longitudinal behavior is examined. These aircraft could be expected to behave similarly to conventional fixed-wing aircraft in the lateral-directional modes.

For trimmers mounted on the wingtips aft of the wing hinge axis, both longitudinal and lateral-directional behavior is examined. Lateral control is assumed to be exercised through differential deflection of the left and right trimmer surfaces. Two forms of aft trimmers are investigated. In one, the two trimmers are allowed freedom to respond independently to local airflow direction changes as well as control tab displacement; in the other, trimmer angular displacement is permitted only by direct pilot command.

In all cases, the left and right wing panels are constrained to symmetrical pitching motion, with no differential wing panel displacement permitted.

SYMBOLS

\bar{C}	mean aerodynamic chord, meters (feet)
C_{Lc}	trimmer lift coefficient
C_{LW}	wing lift coefficient
C_{LMAX}	maximum lift coefficient
Ch_{α}	derivative of trimmer hinge moment coefficient with respect to angle of attack
Ch_{δ}	derivative of trimmer hinge moment coefficient with respect to trimmer angular deflection
$C_{m_r\beta}$	derivative of right trimmer pitching moment coefficient with respect to sideslip angle
C_R	root chord of wing, meters (feet)
D_y	lateral path displacement, meters (feet)
$F_{\substack{x \\ c \rightarrow b}}, F_{\substack{z \\ c \rightarrow b}}$	components of force transmitted from free trimmer to boom, newtons (pounds)
$F_{\substack{x \\ w \rightarrow f}}, F_{\substack{z \\ w \rightarrow f}}$	components of force transmitted from wing to fuselage, newtons (pounds)
L_{Pw}	wing contribution to roll damping coefficient
L_{β}	rolling moment coefficient due to sideslip
M_{R_p}	pitching moment coefficient on right trimmer due to roll rate
$M_{R_{\beta}}$	pitching moment coefficient on right trimmer due to sideslip

N_{Pw}	wing contribution to the yawing moment due to roll rate
N_r	yaw damping coefficient
N_β	yawing moment coefficient due to sideslip
S	wing reference area, meters ² (feet ²)
S_c	free-trimmer reference area, meters ² (feet ²)
U_0	equilibrium true airspeed, meters/second (feet/second)
u	increment in airspeed divided by equilibrium airspeed
V_g	vertical gust velocity, meters/second (feet/second)
X'_{CH}	distance of free-trimmer hinge forward of wing hinge, meters (feet)
α_c	angle of attack of free-trimmer surface, radians
α_F	angle of attack of fuselage assembly, radians
α_W	angle of attack of wing, radians
β	sideslip angle, radians
β_g	sideslip angle caused by lateral gust, radians
δ_a	asymmetric trimmer control tab displacement, radians
δ_c	angular displacement of trimmer with respect to wing, radians
δ_p	angular displacement of wing with respect to fuselage, radians
δ_t	symmetric trimmer control tab displacement, radians
θ	pitch angle of fuselage with respect to horizon, radians
λ	Laplace operator, 1/sec
σ_{nz}	rms normal load factor response, g's
ϕ	roll angle
$\dot{\phi}_g$	rolling gust velocity, per second

PROCEDURE

Mathematical Models

Longitudinal equations. The linearized equations of longitudinal motion are derived in reference 8 and are listed in appendix A of this report. The only modification for the current study was an additional wing pitch damping term which arises for sweep angles other than zero. The additional term follows from the methodology used to model the unsteady lift phenomena. The development of the linear approximations for the unsteady lift of swept wings is given in appendix B.

The longitudinal system has five degrees of freedom. Three variables are required to define the spatial position and orientation of the fuselage in the vertical plane, and two additional variables are required to define the angular displacements of the wing and trimmer surfaces. With unsteady aerodynamic effects included for both lifting surfaces, the linear longitudinal system is of tenth order.

The linearized set of equations describing the longitudinal motion of the aircraft in response to vertical gust velocities and control tab displacement is given by the following equation:

$$[A] \bar{X} = [B] \delta_t + [C] \frac{v}{U_0} \quad (1)$$

Where [A] is a 13 by 13 matrix of the coefficients of the homogeneous equations, and [B] and [C] are column matrices.

The state variable \bar{X} has 13 components: $\alpha_c, C_{L_c}, \delta_c, F_{x_{c \rightarrow b}}, F_{z_{c \rightarrow b}}, \alpha_w, C_{L_w}, \delta_p, F_{x_{w \rightarrow f}}, F_{z_{w \rightarrow f}}, \theta, u,$ and α_F .

Since the system has five independent degrees of freedom, it would have been possible to combine most of the equations to arrive at a set using only five independent variables. These would logically have been $u, \alpha_F, \theta, \delta_p,$ and δ_c . Unfortunately, the elimination of the eight remaining variables involves considerable algebraic manipulation which would have obscured the physical significance and origins of the individual terms in the final equations. The 13 equations were retained as they were derived.

Lateral-directional equations. The lateral-directional equations were used as they were derived in reference 2. Aside from lateral control inputs, the lateral-directional motion of the aircraft system was permitted to be disturbed by spanwise gradients of vertical gust velocity and by lateral gust velocities and gradients. Mathematically, the disturbances appear as rolling gusts and sideslip gusts as shown in the following equations:

$$[E] \begin{bmatrix} \phi \\ \psi \\ \beta \\ \delta_p \\ \delta_a \\ D_y \end{bmatrix} = \begin{bmatrix} -L_{Pw} \\ -N_{Pw} \\ 0 \\ -M_{Rp} \\ 0 \\ 0 \end{bmatrix} \dot{\phi}_g + \begin{bmatrix} -L_\beta \\ -N_\beta - N_r \lambda \\ -Y \\ -M_{R\beta} \\ 0 \\ 0 \end{bmatrix} \beta_g \quad (2)$$

The first three of the equations of this set, given in expanded form in appendix A, are very similar to the ordinary rolling, yawing, and lateral translation equations of a conventional aircraft. The fourth equation, as derived in reference 2, described the pitching motion of the right wing panel. A separate equation for the left panel was not required since it can be shown to be equal in magnitude but opposite in sign to the right panel deflection for small perturbations in the lateral-directional variables. Since the wing panels themselves were not permitted differential displacement in the current study, it was necessary only to redefine the fourth variable to represent the displacement of the right tip trimmer.*

The fifth equation permits the use of closed-loop control of aileron (asymmetric trimmer control tab displacement) in response to bank angle and roll rate, but this feature was not used in this investigation. The last equation is the kinematic relationship for lateral path displacement.

With no feedback to lateral control, the lateral-directional equations represent a sixth order dynamic system.

*The assumption of purely asymmetric trimmer displacement in response to side-slip perturbations is not entirely rigorous for trimmers mounted aft of the wingtips because of possible wing-wake effects on the leeward trimmer. This effect is neglected in this study.

Aerodynamic and mass parameters. Equations (1) and (2) required the estimation of numerous aerodynamic and inertial parameters. The estimation procedures are outlined in appendix C.

Conceptual Aircraft Designs

In this study, attention was confined to wing and trimmer variations of the hypothetical light aircraft used in reference 8. Figure 2 is a multi-view drawing of the baseline aircraft fitted with a straight wing and aft free trimmer. All other configurations were derived by varying the wing sweep angle, the placement of the trimmer (either forward or aft of the wing hinge), or both. The fuselage/tail assembly was kept unchanged throughout.

The basic mission for sizing is fair weather training. Payload is similar to existing aircraft in this mission category and includes two crew and enough fuel for a 3-hour flight. Gross weight is in the 680-kilogram (1500-pound) class. Other features are two-place side-by-side seating ahead of the wing, a shoulder wing, typical general aviation wing loading, an 86 kilowatt (115-BHP) engine in a pusher arrangement, and 20 percent full-span flaps.

Handling Qualities Criteria

Handling qualities criteria were based upon the requirements of the revised military handling qualities specification, MIL-F-8785B(ASG), as given and discussed in reference 9.

For longitudinal analysis, primary attention was given the behavior of the longitudinal short-period modes for stick-fixed motion. Compliance with the standards was determined by examining the characteristic roots of the system of equations. In some instances, the static trim characteristics, both stick fixed and stick free, were also explored.

For lateral-directional motion, the characteristic roots were used to check compliance with dutch-roll damping requirements, roll mode time-constant specifications, and permissible rates of divergence in the spiral mode. Transient motions following abrupt lateral control deflection were also evaluated.

Responses to Atmospheric Turbulence

The responses of the aircraft to continuous atmospheric turbulence were computed using the power spectral density techniques outlined in appendix D.

For comparison purposes, the rms values of selected variables were computed from truncated spectra which eliminated all harmonic components below a temporal frequency of 0.3 radian per second. These low-frequency dis-

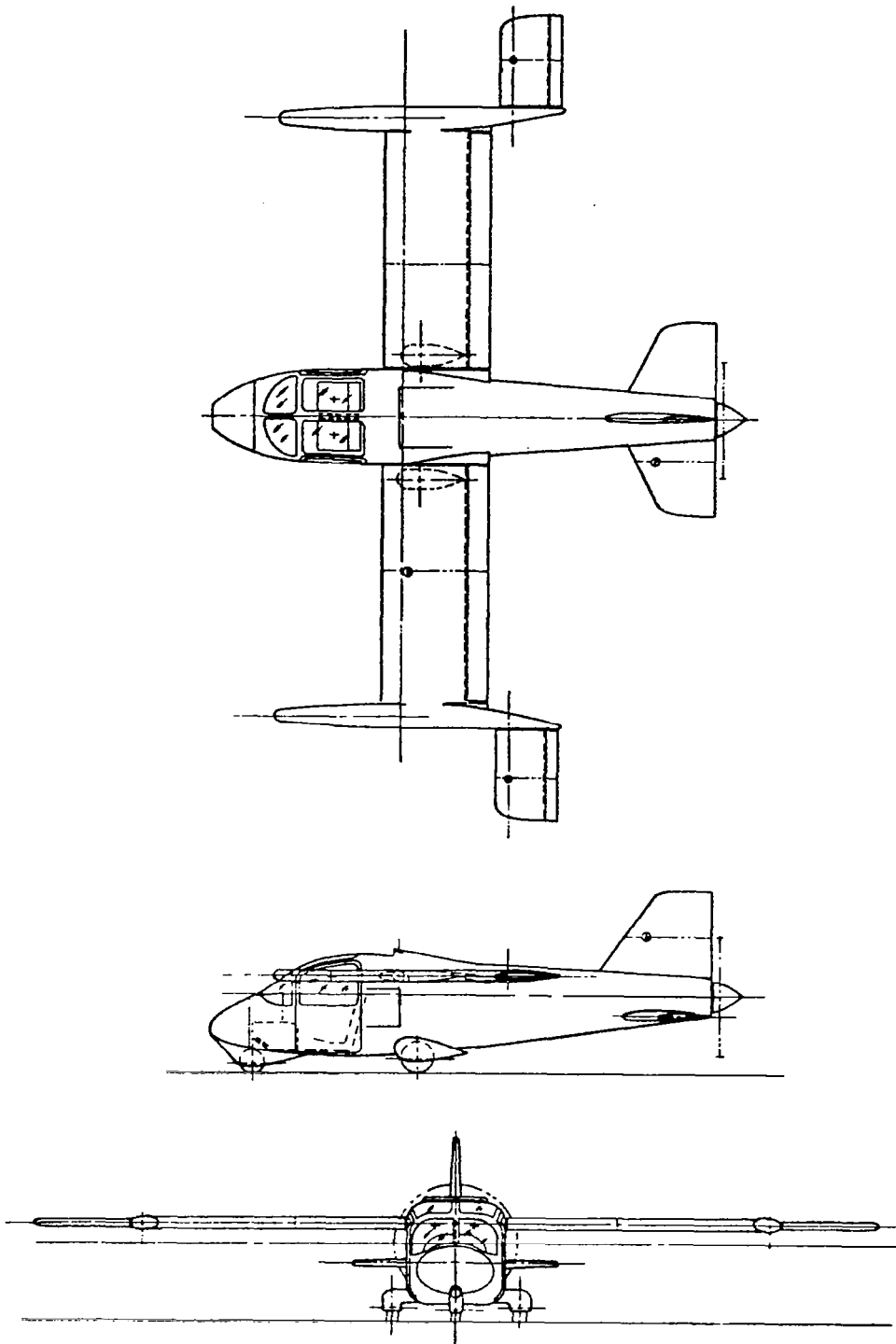


FIGURE 2. BASELINE LIGHT AIRCRAFT WITH STRAIGHT FREE WING AND AFT TRIMMER

turbances are easily controlled by pilot action, and in some cases, a static instability of the spiral mode would have rendered the output spectrum meaningless at zero frequency.

For longitudinal disturbances, only vertical gust components were considered, and the continuous turbulence analysis was augmented, in some cases, by a discrete gust technique to examine the details of an encounter with an isolated gust disturbance.

For lateral-directional motion, the combined effects of uncorrelated rolling and side gusts were computed.

DISCUSSION OF RESULTS

Forward Trimmer Configurations

Results of previous study. At the beginning of the previous free-wing/free-trimmer study, reference 8, the expectation was that the forward trimmer (canard) configuration would prove most deserving of further development for two reasons: (1) canard trimmers could be designed to provide very powerful trimming moments to permit large wing flap deflections, while requiring relatively small ballast weight for mass balancing about the hinge axis; and (2) the trimmer lift is in an upward direction, thereby providing a positive contribution to total airplane lift.

The baseline forward trimmer configuration used in the analysis of reference 8 is shown in figure 3. It featured a trimmer surface area of $1/6$ the wing area, and a moment arm (wing hinge to trimmer hinge) of two wing chord lengths. Trimming power was sufficient to permit a total trimmed airplane lift coefficient (based on wing area) of about 2.6, assuming leading-edge slats and 20 percent full span flaps on the wing.

Unfortunately, the configuration of figure 3 was found to have poor turbulence response characteristics and unacceptable dynamic response behavior to longitudinal control inputs. The rms load factor response to continuous turbulence was, in fact, inferior to an equivalent fixed-wing aircraft - thereby completely negating one of the expected advantages of the concept.

An explanation of the poor turbulence response behavior may be found in the discrete gust encounter plotted in figure 4, from reference 8, wherein the forward-trimmer configuration is compared to a pure free-wing version, with no external trimmer, and corresponding fixed-wing aircraft. All three were subjected to the standard 25 chord-length 1-cosine gust disturbance shown at the bottom of the figure. In the pure free-wing version, the wing begins to deflect almost immediately after encountering the gust, thereby limiting the load factor response to the relatively low value shown in the upper trace. In contrast, the forward trimmer surface experiences an initial upward transient lift force before its downward pitching motion can relieve the load. The transient trimmer force, though lasting less than one-fifth

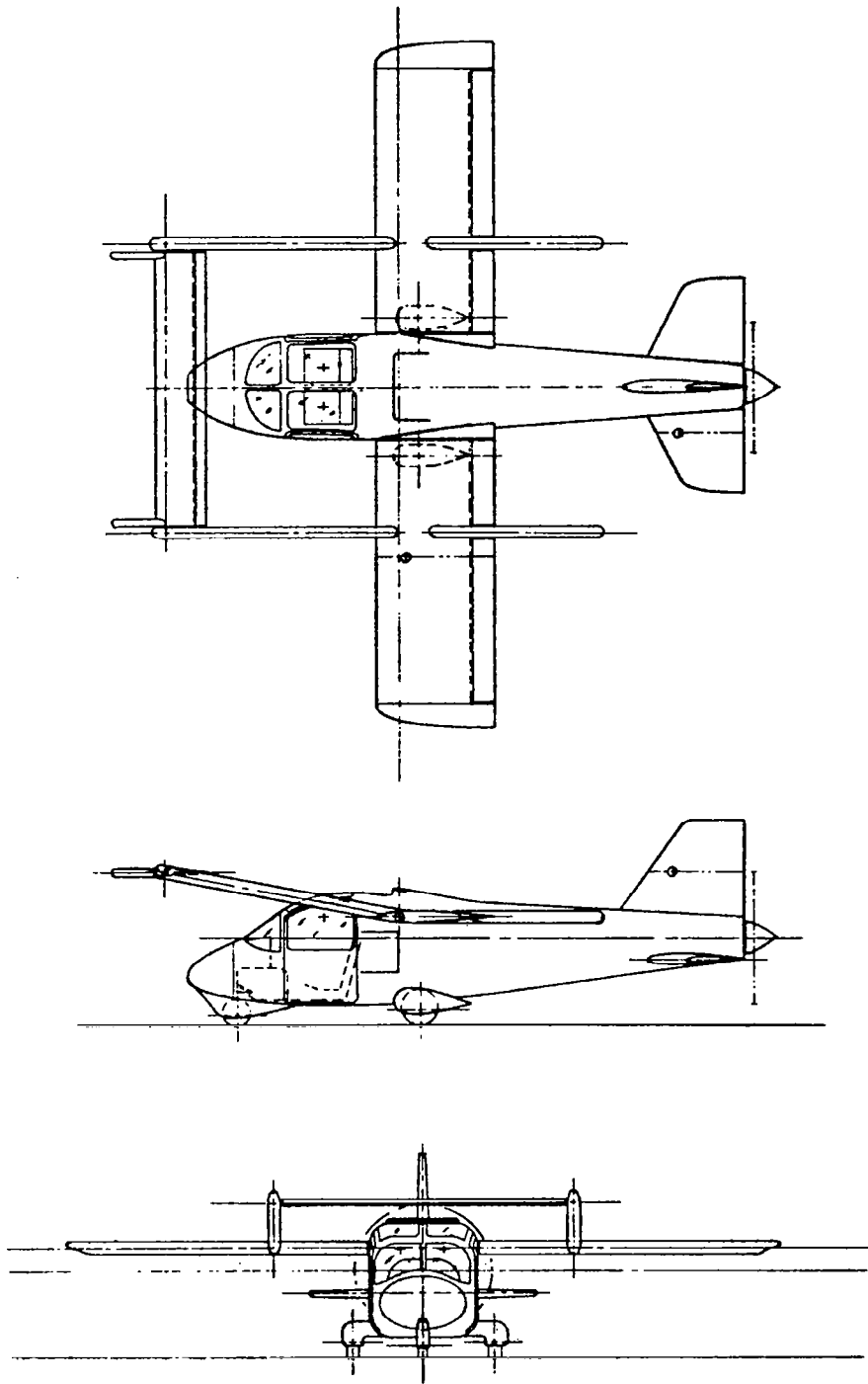


FIGURE 3. FORWARD TRIMMER CONFIGURATION FROM REFERENCE 8

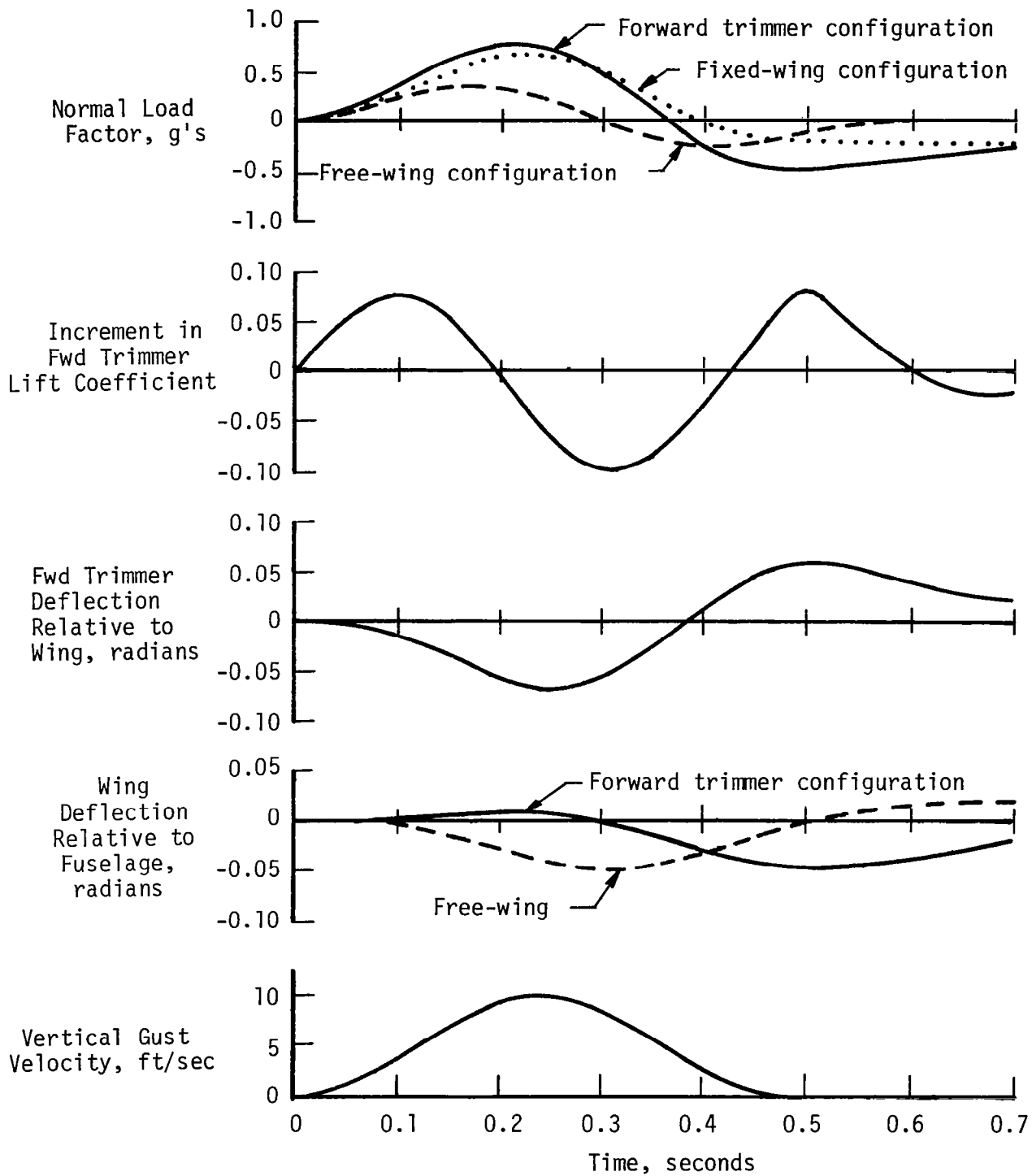


FIGURE 4. VERTICAL GUST RESPONSES ILLUSTRATING ADVERSE TRANSIENT EFFECT OF FORWARD TRIMMER

of a second, imparts a pitch-up impulse to the wing assembly which not only delays the alleviating motion of the wing, but actually produces a small wing displacement in an adverse direction. In the case shown, the wing does not begin to pitch downward until the gust has already passed its peak value.

A simple explanation of the unacceptable control response dynamics is more elusive. Previous studies (refs. 2 and 3) showed that free-wing aircraft exhibit two longitudinal short-period modes, as opposed to the single mode of a conventional airplane. For pure free-wing aircraft, the two short period modes are widely separated in frequency and well damped, causing little interaction between the two. One mode was apparent in the wing pitching motion and the other was largely confined to fuselage pitching. For the free-wing/free-trimmer configuration of figure 3, on the other hand, one of the short-period modes was only very lightly damped and appeared in the motions of both the fuselage and wing/trimmer assemblies.

In seeking improved behavior, shorter moment arms were tried, with the trimmer area held constant. In all cases, examined in reference 8, the dynamic characteristics of the forward trimmer configurations were inferior to aft trimmer arrangements of equal trimmer area and moment arm.

Motivation of current study. In reference 8, the fore and aft trimmer configurations were compared on the basis of constant trimmer area. In view of the inherent weight and maximum lift advantages of forward trimmer arrangements, a portion of the current study was devoted to a reassessment on the basis of equal maximum lift capability. This is a more equitable comparison and permits smaller trimmer volumes for the forward configurations.

Candidate configurations. For comparative purposes, three forward trimmer configurations were selected, each of which can yield the same trimmed $C_{L_{max}}$ as the baseline aft trimmer arrangement of figure 2. The candidate wing/trimmer geometries are shown schematically in figure 5 for three wing sweep angles. In all cases, the wing and total trimmer aspect ratios are held constant at a value of 6.

Although the maximum trimmed lift coefficient capability is identical for each of the arrangements of figure 5, the magnitude of $C_{L_{max}}$ depends upon the selection of high-lift devices on the wing and trimmer surfaces. These values are listed in table 1.

The wing is assumed to use an NACA 23012 airfoil section with a full-span 20 percent slotted flap; and, in the latter two cases, with a Handley-Page leading-edge slat. This selection was based on the availability of pertinent data, and the trimmed lift capability was estimated using the procedure described in reference 8.

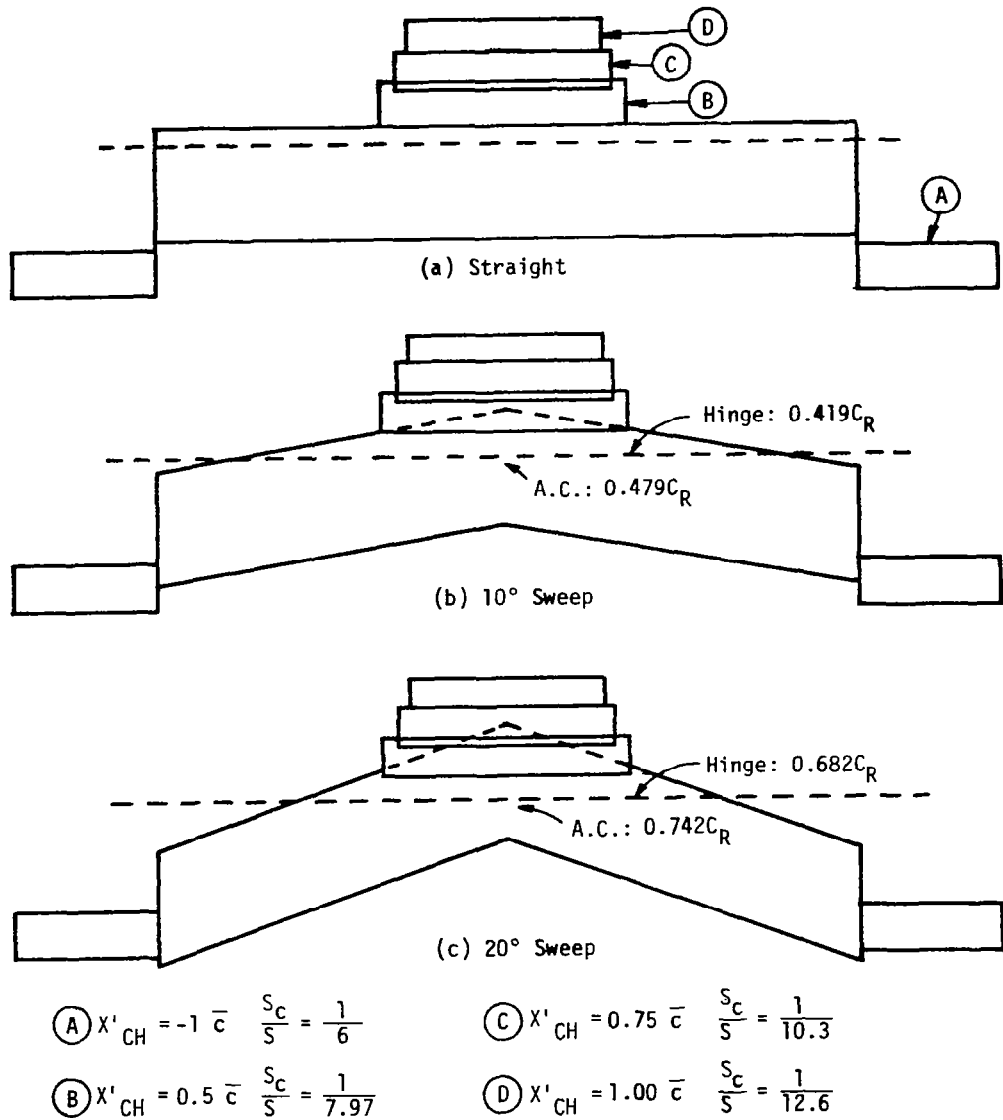


FIGURE 5. FREE-TRIMMER CONFIGURATIONS YIELDING THE SAME TRIMMED C_{LMAX}

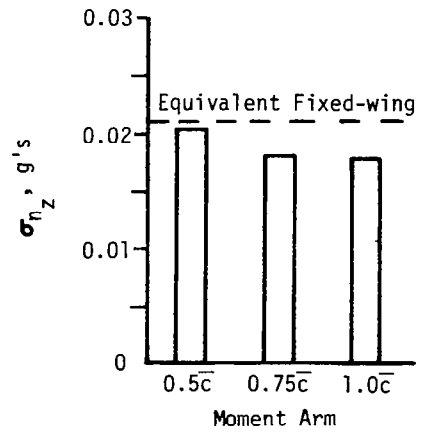
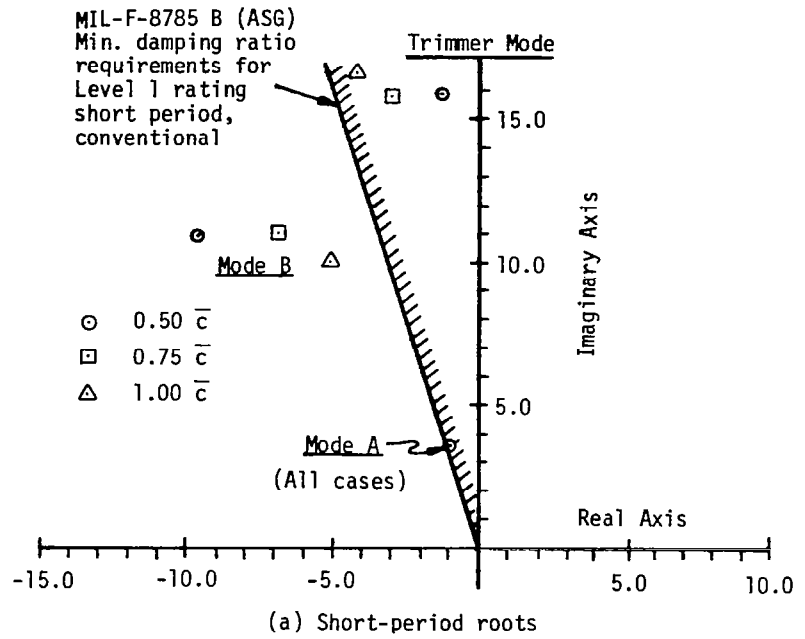
TABLE I. TRIMMED $C_{L_{MAX}}$ OF CANDIDATE CONFIGURATIONS

High-Lift Devices	$C_{L_{MAX}}$
1. Wing Flaps, Plain Trimmer	1.27
2. Wing Flaps, L.E. Slat on Trimmer	1.41
3. Wing Flaps + L.E. Slat, Plain Trimmer	1.64
4. Wing Flaps + L.E. Slat, L.E. Slat on Trimmer	1.75

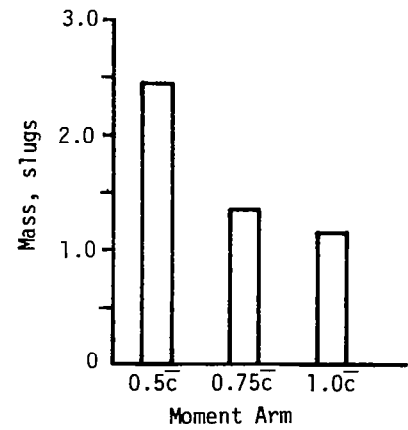
Comparison of forward-trimmer configurations. As reported in reference 8, the dynamic characteristics of free-wing/free-trimmer aircraft generally consist of four oscillatory modes. One of these modes is the long-period phugoid oscillation, which differs little from a more conventional aircraft. For this reason, and to conserve computer time during this analysis, the air speed degree of freedom was removed from the set of longitudinal equations (eq.(1)). This simplification has a negligible effect on the remaining modes because the phugoid frequency is much lower than the rest. Furthermore, with the phugoid eliminated, continuous turbulence responses do not contain large contributions at the low phugoid frequencies, which are easily attenuated by pilot action.

With the phugoid eliminated from further consideration, three oscillatory modes remain. One of these is a high frequency mode which is related to the pitching of the trimmer about its hinge axis. The other two are dual short-period modes which dominate the motion of the wing and fuselage assemblies. These are the modes of primary interest.

In comparing the three candidate forward trimmer configurations, three criteria were used: the modal roots; the rms load factor response to continuous turbulence; and the mass of the booms and counterweights required to support the trimmer and to achieve mass balance about the wing hinge axis. These are compared graphically in figure 6. The roots and turbulence responses were computed for cruise flight of 241.4 kilometers per hour (150 miles per hour) at an altitude of 1829 meters (6000 feet). The fuselage center of gravity was 0.762 meters (2.5 feet) directly below the wing hinge.



(b) RMS load factor response to unit turbulence intensity



(c) Mass of booms & counterweights

FIGURE 6. COMPARISON OF CANDIDATE FORWARD TRIMMER CONFIGURATIONS

For a conventional light aircraft in cruise flight, MIL-F-8785B(ASG) requires a minimum short-period damping ratio of 0.3 for the highest level of acceptability, Level 1. Mode A very nearly meets the standard, as seen in figure 6(a), whereas Mode B roots exceed the requirement by a wide margin for all three cases. The mode A roots, which are primarily related to fuselage motion, are not noticeably influenced by the choice of trimmer configuration when plotted on the scale of figure 6(a).

For completeness, the trimmer mode roots are also shown in Figure 6(a). The trimmer roots are of higher frequency and, in these cases, are more lightly damped than either mode A or mode B. Yet, there is no obvious reason to require the trimmer mode damping, per se, to meet the conventional short-period standards, since this mode would not be directly apparent to the pilot except for its influence on the wing motion, which is dominated by mode B.

It should be mentioned at this point that the direct and literal application of the conventional short-period standards of MIL-F-8785B(ASG) is open to question. There are two primary reasons for uncertainty with regard to the validity of the application. These are: (1) the standards assume a single, second-order, short-period mode, whereas two would be apparent to the pilot of these aircraft, and one of these may be influenced by yet a third (the trimmer mode) and (2) the phasing between fuselage pitch acceleration and normal load factor build-up, in response to control input, is substantially different than a conventional airplane.

With regard to turbulence response, in figure 6(b), the $1.0\bar{C}$ case is superior, although only slightly better than the $.75\bar{C}$ arrangement.

The greatest advantage of the $1.0\bar{C}$ configuration is in the reduction of weight, as shown in figure 6(c). In fact, for the $1.0\bar{C}$ moment arm case, the wing/trimmer assembly is very nearly balanced about the wing hinge solely by the mass of the trimmer and booms, with no additional ballast required. A longer moment arm, with reduced trimmer area to maintain the constant trimmed lift capability, would require ballast weight aft of the wing hinge.

On the basis of the comparison factors shown in figure 6, the forward trimmer configuration with the $1.0\bar{C}$ moment arm and area ratio of 1/12.6 was selected for further analysis and for comparison with aft trimmer arrangements. The complete configuration is shown in figure 7.

Control response characteristics. Control response behavior was investigated by computing the time history of an abrupt pull-up maneuver for the aircraft of figure 7. A step deflection of the trimmer control tab was sized to establish a peak load factor increment of $1g$. The time history is shown in figure 8. For the time-history computation, all degrees of freedom were retained, including airspeed.

Figure 8 illustrates the previously mentioned bimodal character of the normal load factor response. The early part of the response, up to about

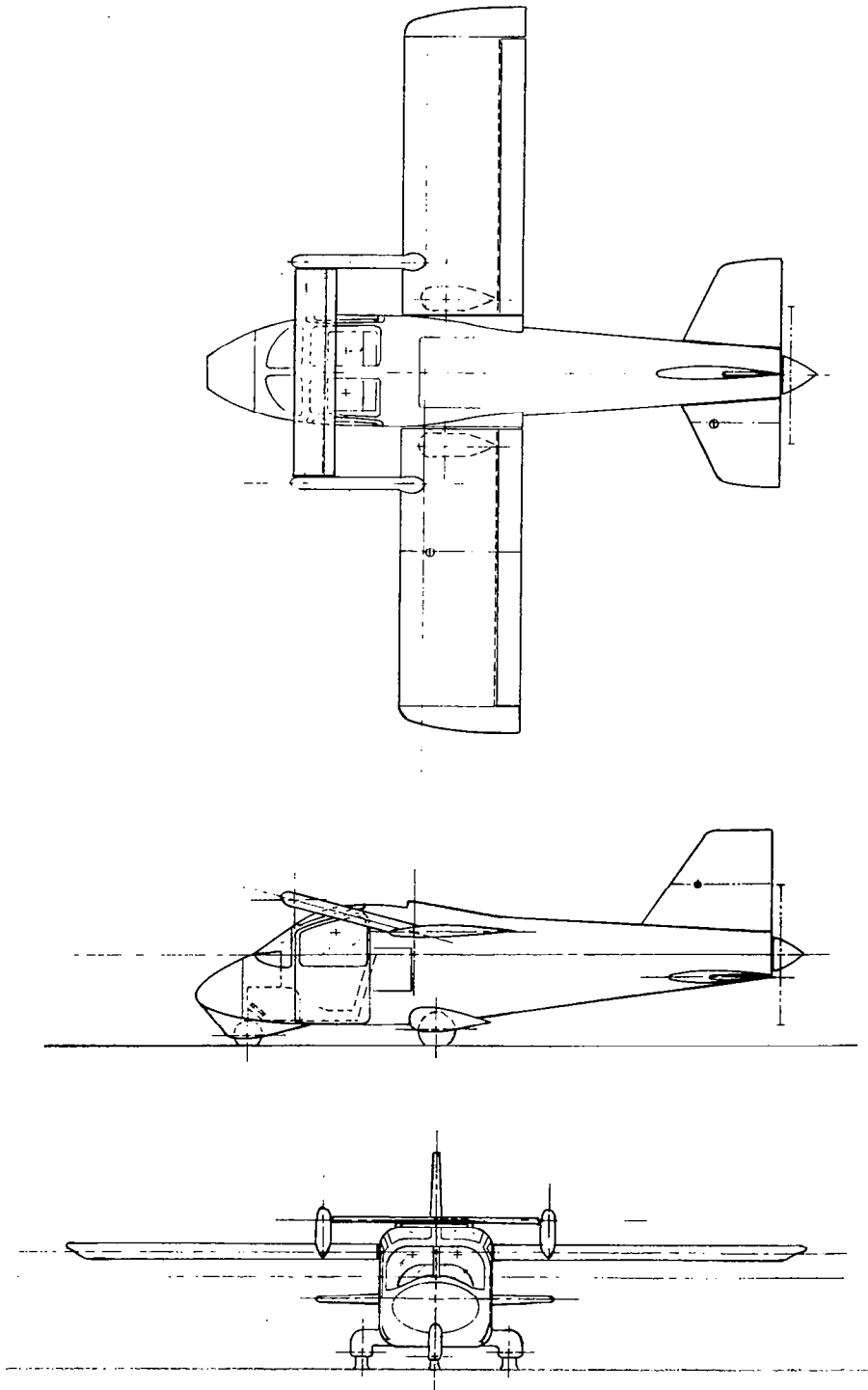


FIGURE 7. SELECTED FORWARD TRIMMER CONFIGURATION

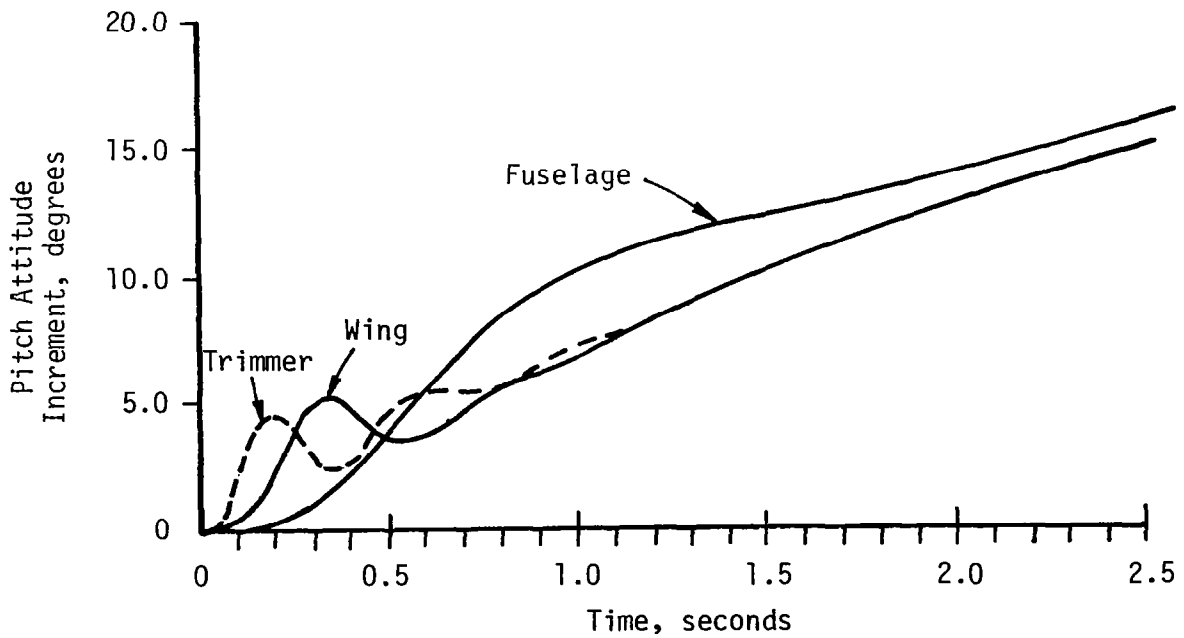
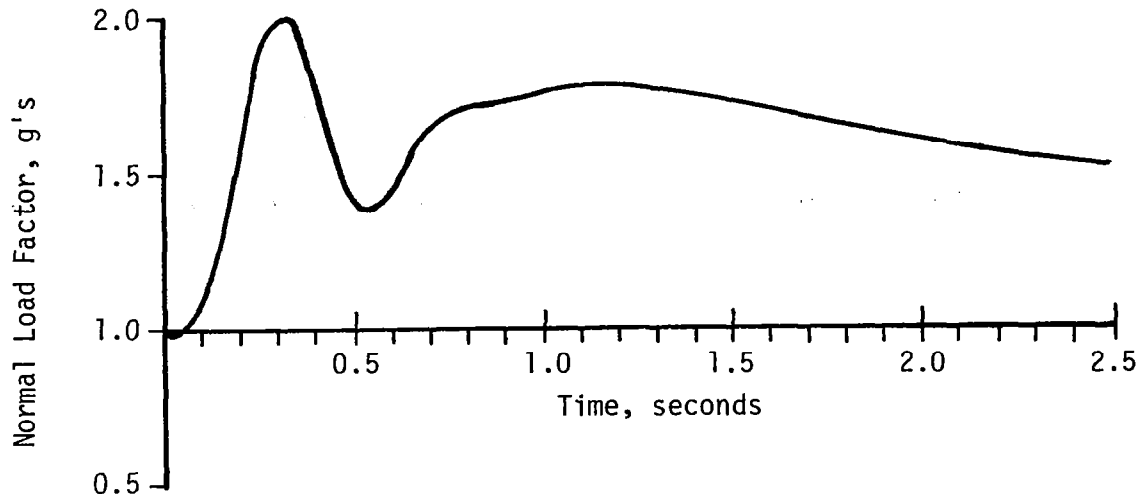


FIGURE 8. RESPONSE TO STEP LONGITUDINAL CONTROL INPUT, FORWARD TRIMMER/STRAIGHT WING, CRUISE

1 second, is dominated by mode B, which is apparent in the wing pitching motion in the lower trace; the latter part displays the lower frequency character of mode A and the beginning of the phugoid oscillation. On the other hand, the fuselage pitching motion cannot respond at the mode B frequency and is totally dominated by mode A.

The shape of the normal load factor trace appears to be less than ideal during the early transient stage, but it is difficult to predict the acceptability of the rapid overshoot and undershoot which is evident. Existing handling qualities specifications offer little guidance in this case because of the unorthodox dichotomy between load factor and fuselage pitching. The rapidity of the acceleration transient, coupled with the smoothness of the fuselage pitching motion, might serve to mask the transient behavior from the pilot.

Effect of wing sweep. Prior to this study, it was felt that a swept wing might offer certain structural advantages by reducing the length of external supporting booms for the trimmer surfaces. For tip mounted aft trimmers, an advantage does exist, as will be discussed later in this report. For forward trimmers, on the other hand, the wing sweep creates an additional weight penalty. In the first place, the requirement for static balance about the wing hinge generally dictates a forward-placed mass in excess of the weight of the supporting booms. Secondly, with a swept wing, the center of gravity of the free portion of the wing (excluding the center section which is immersed in the fuselage) moves aft slightly with respect to the aerodynamic center.

Nevertheless, the dynamic behavior of forward trimmers with swept wings was examined. Wing sweep angles of 10 deg and 20 deg were explored, as shown in figure 5. Table II compares the characteristic roots, turbulence responses, and weight penalties for the three sweep angles.

No dramatic changes are seen for the range of wing sweep angles which were considered. On the beneficial side, the damping ratio of mode A is improved with wing sweep, as is the turbulence response. On the negative side, the weight penalty is significant and the frequency and damping ratio are somewhat reduced for mode B, probably as a result of an increased wing pitching moment of inertia.

Aft Trimmer Configurations

Results of previous study. With the constant trimmer area ratio considered in reference 8, the tip-mounted aft free-trimmer arrangement of figure 2 had been selected as the most promising free-wing/free-trimmer configuration. The longitudinal control responses appeared to be good and gust alleviation was excellent, being virtually identical to that of a pure free-wing aircraft of equivalent design, but without the external trimmers. On the adverse side, the weight penalty for balance about the wing hinge was substantially greater than the forward trimmer concept.

TABLE II. EVALUATION CRITERIA FOR FORWARD TRIMMER CONFIGURATION WITH THREE WING SWEEP ANGLES

$$\frac{S_c}{S} = 1/12.6$$

Cruise Flight

	Wing Sweep Angle		
	0 deg	10 deg	20 deg
Mode A Roots	-1.04 + j 3.63	-1.13 + j 3.68	-1.42 + j 3.81
Mode B Roots	-5.04 + j 10.01	-4.08 + j 8.75	-2.91 + j 7.26
RMS Load Factor, Unit Turbulence Intensity	0.0178	0.0166	0.0152
Mass of Booms and Counter- weights	1.18	1.45	2.02

Rationale of current study. Unlike the forward trimmers, the tip-mounted aft trimming surfaces could be expected to have a significant effect on the lateral-directional behavior of the aircraft. Furthermore, their outboard location suggests their use for lateral control, permitting the use of one-piece, full-span flaps on each wing panel. For these reasons, a primary objective of the current analysis was to extend the study of these configurations to include the lateral-directional handling qualities and turbulence responses.

As an additional subject, the current study explored the potential merits of tip trimmers which are directly controllable by the pilot, but which are not free to rotate about their hinge axis in response to local air-flow direction. The motivation here is the fact that a "fixed" trimmer would, unlike the free trimmer, cause a rearward shift in the aerodynamic center of the wing/trimmer combination. This would permit moving the wing hinge axis aft and would reduce the weight penalty for balance about the wing hinge.

Free aft-trimmer capabilities. By design, the maximum trimmed lift capability of the free aft trimmer is identical to the forward-trimmer configurations previously discussed. The maximum lift depends upon the selection of high-lift devices on the wing and trimmer surfaces and varies from 1.27 to 1.75 as listed in table I.

In all cases, the maximum trimmer power is required when the wing lift is a maximum. The downward trimmer force is always opposed by the wing lift, acting behind the wing hinge, and by the negative moment caused by wing flap deflection. Static stability is assured throughout the attainable lift range.

Fixed aft-trimmer capabilities. If the aft trimmer of figure 5 is not free, the aerodynamic center of the wing/trimmer combination moves aft to about 39.5 percent of the wing chord. To maintain a static hinge margin of 6 percent for consistency with other configurations in this study, the wing hinge can then be moved to 33.5 percent wing chord, which is approximately 8.5 percent of the wing chord aft of the wing-alone aerodynamic center.

With this arrangement, the wing lift produces a positive (leading-edge-up) moment about the wing hinge and the maximum lift coefficient is limited primarily by the wing capabilities rather than trimmer power. As a consequence, the fixed-trimmer configuration has a higher lift potential than the free-trimmer arrangement of the same geometry.

At the same time, it is important to note that this same moment balance has a subtle, but very important, implication for flight safety. In fact, the fixed-trimmer power is designed, not by the maximum desired lift capability, but by the need to prevent a possible uncontrolled divergence.

The trim characteristics of the straight-wing/fixed-trimmer configuration are shown in figure 9 for the wing with flaps, but no leading-edge slat.

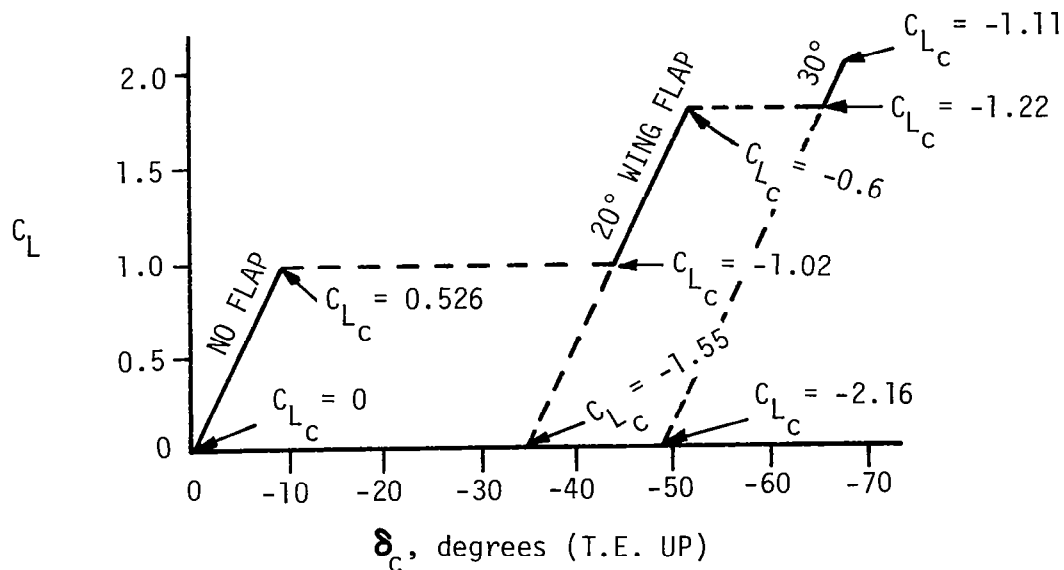


FIGURE 9. TRIM CHARACTERISTICS, STRAIGHT WING/AFT FIXED TRIMMER

With no flap deflection on the wing, the equilibrium lift coefficient of the trimmer becomes increasingly positive as the wing is trimmed to higher lift coefficients. This is in contrast to the free-trimmer case, where larger negative trimmer lift would be required to offset the moment caused by wing lift.

If the wing flaps are deflected, a more negative load is required on the trimmer to counter the flap pitching moment, but the trend to more positive (less negative) trimmer lift remains as the wing is trimmed to higher lift coefficients. As a consequence, for any flap deflection, the greatest demand on trimmer power occurs not at maximum airplane lift, as might be expected, but at the lower airplane lift coefficients.

If it is assumed that an all-moving trimmer with no high-lift devices can provide a maximum lift coefficient of about 1.2, and if the wing flaps were deflected 30 degrees, the data of figure 9 indicate that the trimmer could only provide equilibrium for total airplane lift coefficients in excess of about 1.8. If the wing lift were reduced by a push-over maneuver or by a downward gust, the wing flap moment could produce an uncontrollable divergence in the negative direction which could not be arrested by the trimmer.

To preclude a catastrophic loss of control, the trimmer must be able to balance the most negative lift coefficient attainable by the wing. For the no-flap case, no problem appears, since the maximum negative wing lift would only require a negative trimmer lift coefficient of about 0.526 (assuming the wing maximum C_L is the same for both positive and negative angles of attack). Furthermore, it is fortunate that the maximum negative wing lift is substantially reduced by wing flap deflection. For example, the maximum negative wing lift coefficient with 20 degree flap deflection is estimated to be only about -0.33. To maintain control in this case would require a trimmer lift coefficient capability of about 1.95 for the aircraft under consideration here. Similarly, the most negative wing lift coefficient obtainable with 30 degrees of flap is near zero, which implies a maximum trimmer lift coefficient capability of about 2.2.

It appears that the high trimmer lift requirements are within reason if appropriate high-lift devices are used on the trimmer. Since the trimmer is not free-floating, trailing-edge flaps are not precluded as they are with free trimmers.

Returning to figure 9, the stick-fixed trim characteristics are seen to be satisfactory, since increasing trailing-edge-up deflection is required to trim to higher lift coefficients. The stick-free trim behavior, on the other hand, will only be acceptable if hinge moments caused by angle of attack changes are not fed back to the control system. This is not surprising since the aft wing hinge axis location would lead to a predictable divergence if the trimmer were free to pitch into the local relative wind. The inherent trim force characteristics are not felt to be a difficult problem. A well-established solution would be to pivot the trimmer about its quarter-chord ($C_{h\alpha} = 0$) and rely on an antiservo tab to provide a desirable level of hinge

moment due to surface deflection ($C_{h\delta} < 0$). This scheme has been applied successfully, for example, on the horizontal stabilizer of the Piper Cherokee series.

Longitudinal characteristics of aft trimmers. Figure 10 compares the characteristic roots, turbulence responses and weight penalties for two variations of the aircraft of figure 2. In one case, the trimmers are free floating; in the other, the wing hinge has been moved aft and the trimmers are controllable, but not free.

The damping ratio of the mode A roots, as seen in figure 10(a), does not meet the Level 1 standards of MIL-F-8785B(ASG) for short-period motion, but exceeds the relaxed standards of Level 2. Furthermore, the selection of free or fixed trimmer has very little influence on this mode.

The roots of mode B, primarily associated with the wing assembly, exceed the Level 1 standards for both cases.

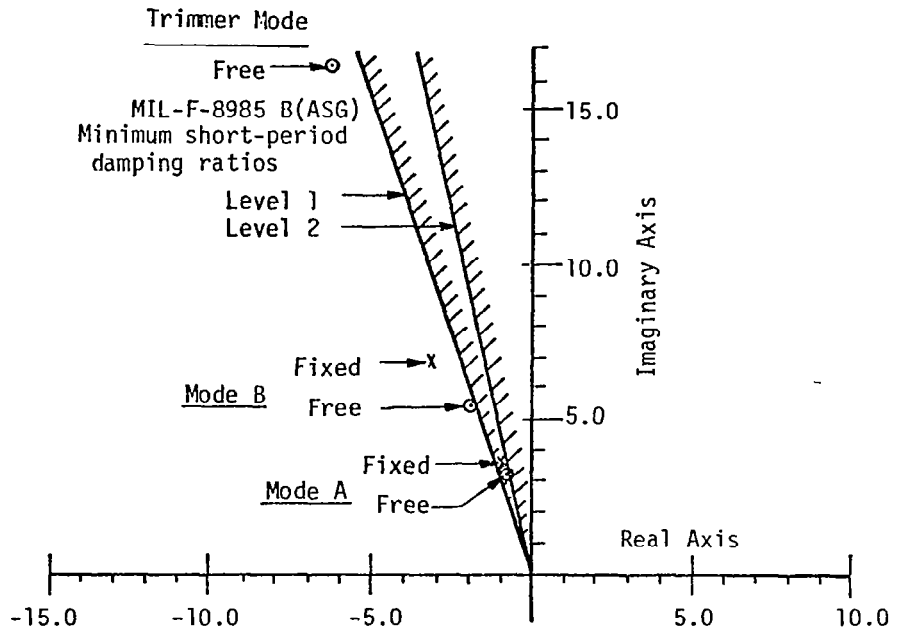
Both trimmer configurations provide excellent gust alleviation, as seen in figure 10(b), but the relative inferiority of the fixed-trimmer arrangement was surprising. It might be expected that the higher natural frequency and slightly better damping of mode B (fig. 10(a)) would cause the fixed trimmer to be superior, but this was not the case. A detailed examination of the response spectra failed to reveal a simple explanation, although the wing pitching response to vertical gusts shows a substantially greater phase lag above the mode B frequency.

Figure 10(c) shows the advantage of the fixed trimmer from the weight penalty standpoint, but even here, the mass of booms and counterweights is approximately four times that of the forward trimmer configuration. It should be emphasized that the absolute magnitudes of the weight penalty are sensitive to several assumptions and only the relative magnitudes should be considered. A precise evaluation of the weight penalties would require a structural design and analysis effort for each particular configuration, and such an effort was beyond the scope of this study.

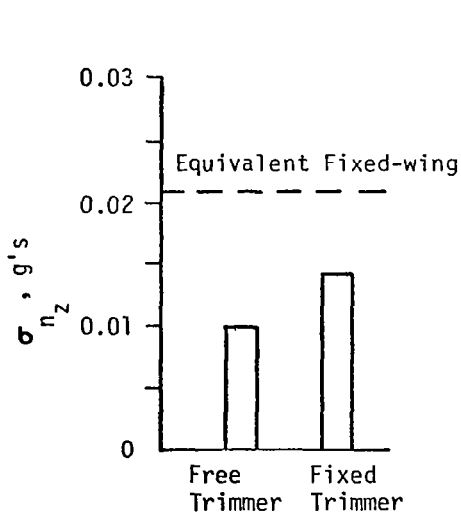
Longitudinal control responses. Time histories of abrupt pull-up maneuvers were computed for both the free and fixed aft trimmers. As in the forward trimmer analysis, the step deflection of the longitudinal control was sized to produce an incremental lg load factor.

Figure 11 shows the response of the free-trimmer configuration. In comparing this response with that of the forward trimmer in figure 8, the noteworthy differences are in the wing transient motion and the fuselage pitching response. The wing transient of figure 8 is not present for the aft trimmer, resulting in a smoother load factor response for the aft free-trimmer arrangement. On the other hand, an increased fuselage motion is evident in figure 11.

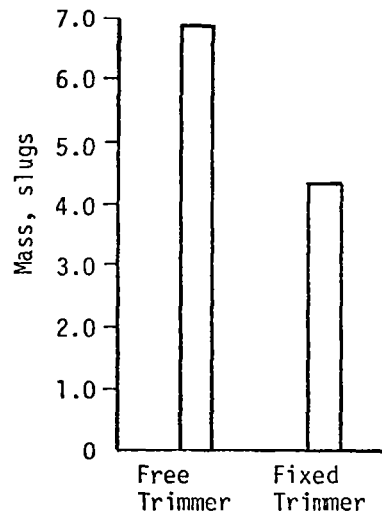
A similar response history is plotted in figure 12 for the fixed aft trimmer. This response is seen to be very similar to the free-trimmer behavior.



(a) Short-period roots



(b) RMS load factor response to unit turbulence intensity



(c) Mass of booms & Counterweights

FIGURE 10. LONGITUDINAL COMPARISON OF FREE AND FIXED AFT TRIMMERS STRAIGHT WING, CRUISE

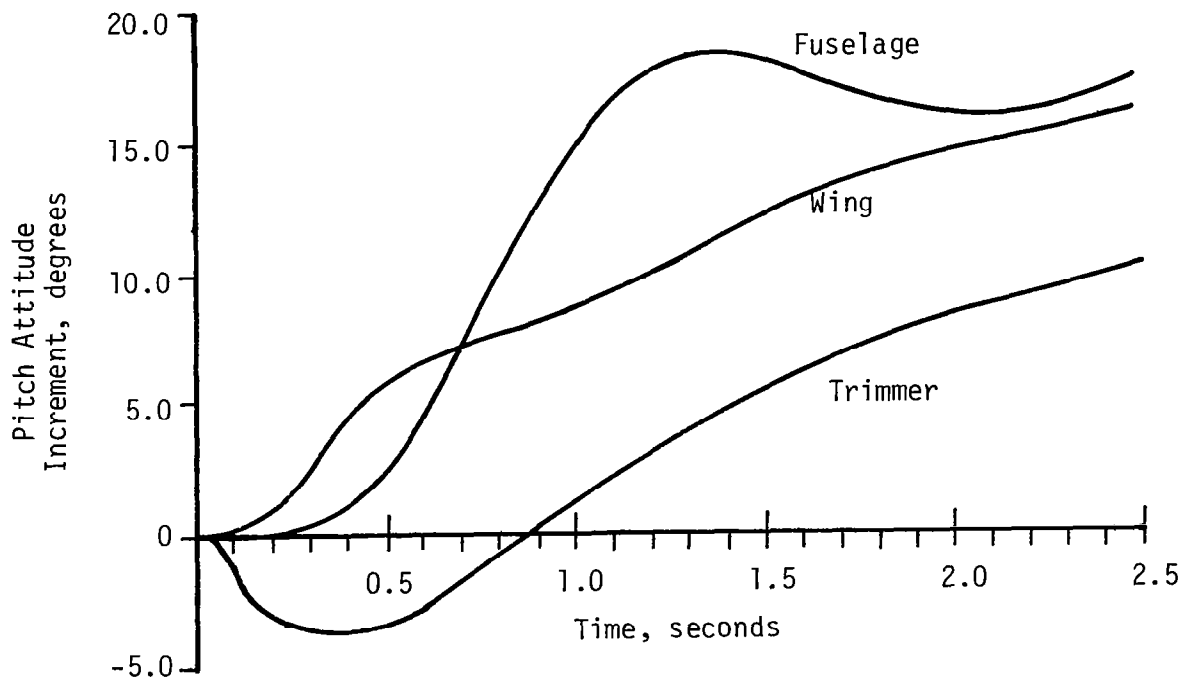
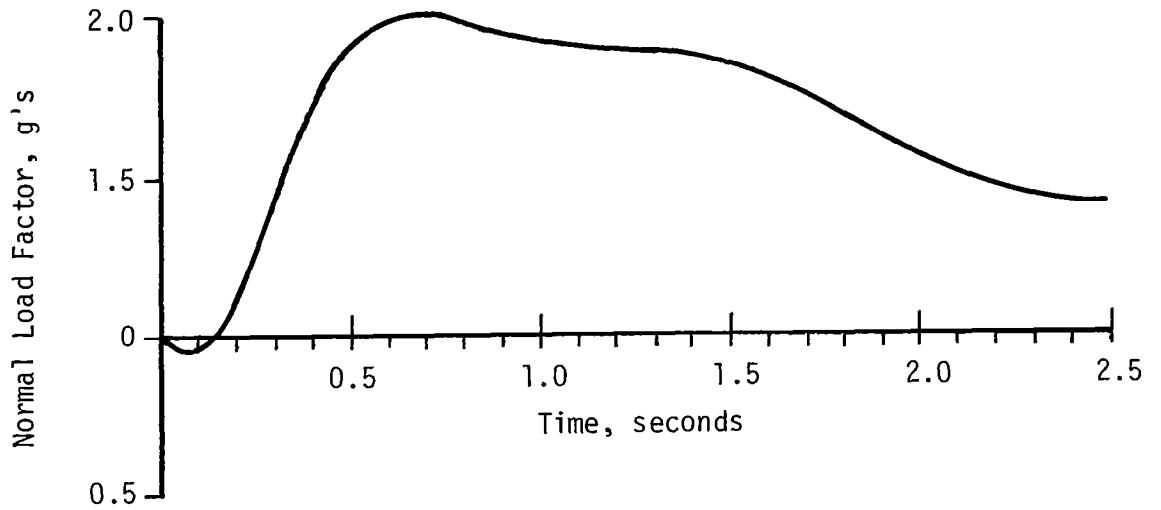


FIGURE 11. RESPONSE TO STEP LONGITUDINAL CONTROL INPUT, FREE AFT TRIMMER/STRAIGHT WING, CRUISE

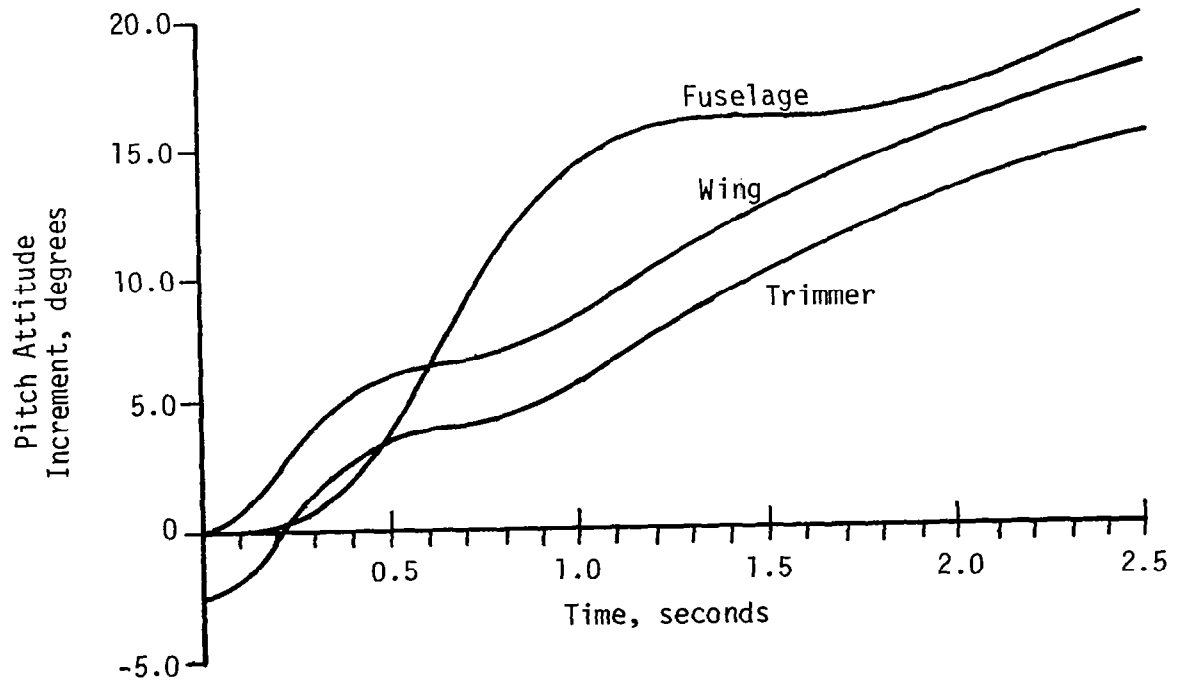
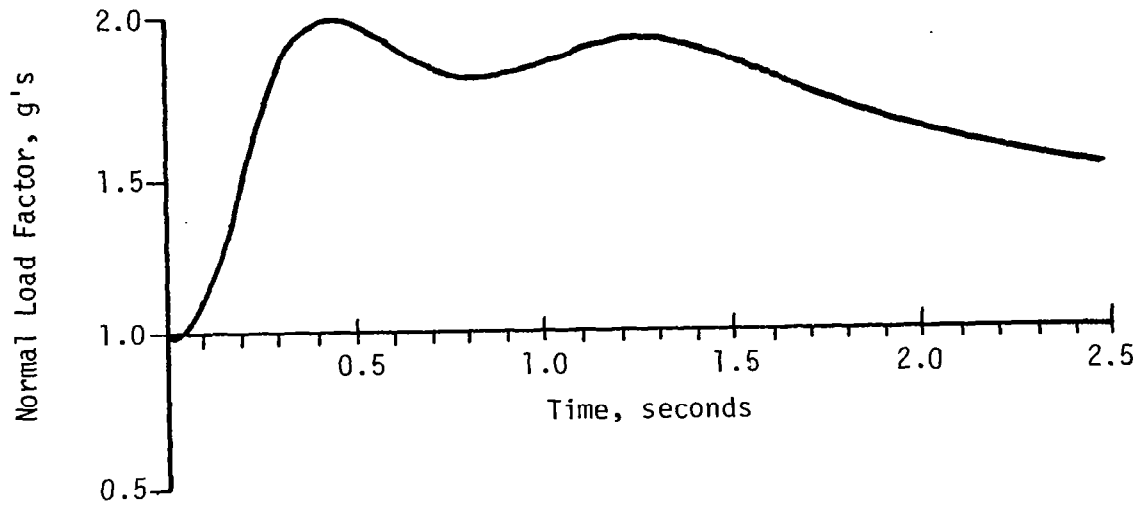


FIGURE 12. RESPONSE TO STEP LONGITUDINAL CONTROL INPUT, FIXED AFT TRIMMER/STRAIGHT WING, CRUISE

In both the free and fixed-aft trimmer responses, the relatively high-frequency damped oscillation of mode B is evident, superimposed on the longer period motion of mode A. In both cases, however, the response histories appear to be satisfactory.

Longitudinal effects of wing sweep angle. Table III compares the evaluation criteria for the free- and fixed-trimmer configurations for the three values of wing sweep angle.

As in the case of the forward trimmer (table II), there are no dramatic effects of sweep angle on the characteristic roots. For the aft trimmers (table III), wing sweep has even less effect on the turbulence response than for the forward trimmer arrangement.

TABLE III. LONGITUDINAL CRITERIA FOR AFT TRIMMER CONFIGURATIONS WITH THREE WING SWEEP ANGLES

CRUISE FLIGHT

	Wing Sweep Angle		
	0 deg.	10 deg.	20 deg.
(a) Free Trimmer			
Mode A Roots	- .673 + j 3.394	- .753 + j 3.45	- 1.08 + j 3.66
Mode B Roots	-1.98 + j 5.45	-2.00 + j 5.44	- 1.61 + j 4.84
RMS Load Factor Unit Turbulence Intensity	.00982	.00963	.00997
Mass of Booms and Counter- weights	6.83	5.73	5.92
(b) Fixed Trimmer			
Mode A Roots	- .793 + j 3.573	- .857 + j 3.67	- 1.04 + j 3.77
Mode B Roots	-3.12 + j 6.91	-3.28 + j 6.29	-3.05 + j 6.64
RMS Load Factor, Unit Turbulence Intensity	.0142	.0147	.0145
Mass of Booms and Counter- weights	4.29	3.45	3.55

On the positive side, about 10 degrees of wing sweep appears to offer a measurable reduction in weight for the aft trimmers. Furthermore, the aft shift of the wingtip with respect to the trimmer surface offers an obvious structural advantage for attaching the trimmer hinge to the wingtip. Figure 13 is a drawing of the complete aircraft with aft trimmer and 10 degrees of wing sweep.

Lateral-directional behavior. The purposes of the lateral-directional analysis were:

(1) To assess the influence of tip-mounted aft trimmers, both free and fixed, on the lateral-directional modes and turbulence responses.

(2) To examine the feasibility of the use of differential trimmer displacement for lateral control.

(3) To determine the effect of fuselage trimmed attitude (deck angle) on the lateral-directional behavior.

The first case examined was the baseline straight-wing configuration of figure 2 with the trimmers free to respond independently to local flow conditions. The roots of the sixth-order set of equations (appendix A) were evaluated for three fuselage deck angles and for two flight conditions: cruise at a true speed of 241.4 kilometers per hour (150 miles per hour), at an altitude of 1829 meters (6000 feet); and approach, at a true speed of 132.8 kilometers per hour (82.5 miles per hour).

Fuselage trim attitude determines the effective product of inertia, I_{XZ} , coupling the roll and yaw accelerations, and also raises or lowers the vertical tail surface with respect to the flight path. The latter effect has a strong influence on the net dihedral effect and on the cross-derivatives C_{ℓ_r} and C_{n_p} . The development of these parameters is outlined in appendix C.

The roots were used to evaluate the dutch roll damping ratio, the rate of divergence of the spiral mode (if unstable), and the roll mode time constant. These criteria were then used to judge the acceptability of the modal characteristics from the standpoint of handling qualities.

The results of the calculations are listed in table IV.

In the terminology of MIL-F-8785B(ASG), this is a Class I airplane, and, in cruise, the flight phase is Category B. For the highest level of acceptability, Level 1, the minimum dutch roll mode damping ratio is 0.08. This criterion is met for the cruise condition, as are other dutch roll criteria; but table IV clearly shows that the dutch roll damping deteriorates as the fuselage is trimmed to negative (nose down) attitudes.

Both the spiral and roll mode characteristics exceed the Level 1 standards of the handling qualities specification. The spiral mode is convergent for all three deck angles and the roll mode time constant is well within the maximum value of 1.4 given by reference 9.

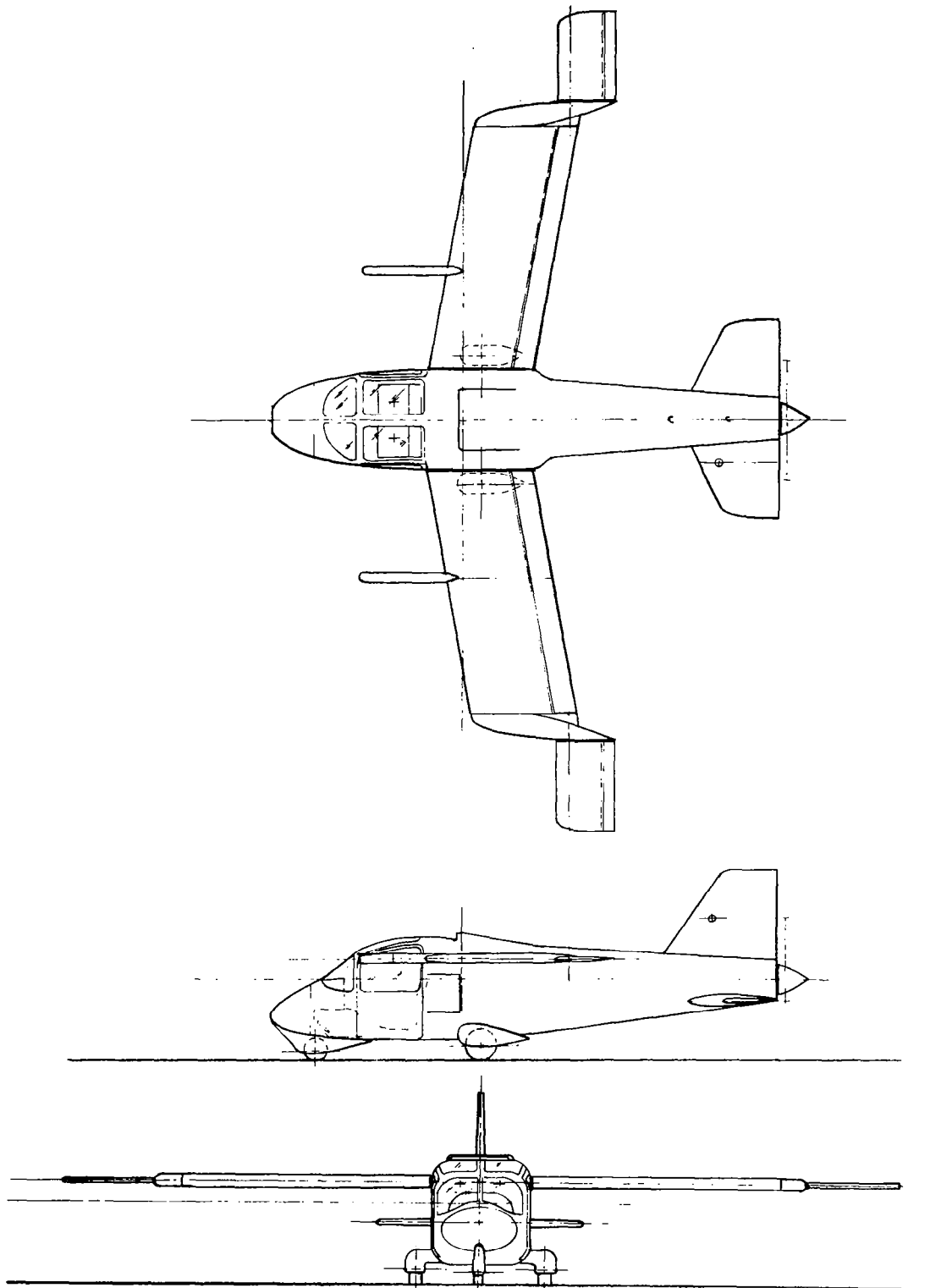


FIGURE 13. AFT TRIMMER CONFIGURATION WITH 10° SWEEP

For the approach condition, the dutch roll damping meets or exceeds the Level 1 standards except for the nose-down fuselage attitude case, which causes the dutch roll mode to become mildly divergent. The spiral and roll mode behavior are well within the Level 1 standards.

The asymmetric trimmer mode listed in table IV is a well damped oscillatory mode which, by virtue of its high frequency, is confined to asymmetric motion of the free trimmers with a negligible effect on the conventional lateral-directional modes.

TABLE IV. LATERAL-DIRECTIONAL CHARACTERISTICS
STRAIGHT WING/FREE AFT TRIMMER

	Fuselage Deck Angle		
	<u>Nose Down</u> - 15 deg	0 deg	<u>Nose Up</u> + 15 deg
(a) Cruise			
Dutch Roll Roots	$-0.241 + j 2.58$	$-0.404 + j 2.94$	$-0.492 + j 3.22$
Dutch Roll Damping Ratio	0.09	0.14	0.15
Spiral Mode Roots	-0.00978	-0.00914	-0.00744
Roll Convergence Roots	-3.20	-2.94	-2.72
Roll Mode Time Constant	0.313	0.340	0.368
Asymmetric Trimmer Mode	$-4.21 + j 16.4$	$-4.25 + j 16.4$	$-4.21 + j 16.4$
(b) Approach			
Dutch Roll Roots	$+0.0102 + j 1.50$	$-0.140 + j 1.74$	$-0.247 + j 1.94$
Dutch Roll Damping Ratio	---	0.08	0.13
Spiral Mode Roots	-0.0537	-0.0444	-0.0335
Roll Convergence Roots	-2.44	-2.22	-2.02
Roll Mode Time Constant	0.410	0.450	0.495
Asymmetric Trimmer Mode	$-2.84 + j 9.96$	$-2.85 + j 9.93$	$-2.81 + j 9.92$

The analysis just described was repeated for the fixed-trimmer case in which the trimmer is not free to respond to the aircraft motion. The results are given in table V.

TABLE V. LATERAL-DIRECTIONAL CHARACTERISTICS
STRAIGHT WING/FIXED AFT TRIMMER

	Fuselage Deck Angle		
	Nose Down - 15 deg	0 deg	Nose Up + 15 deg
(a) Cruise			
Dutch Roll Roots	$-0.325 \pm j 2.77$	$-0.433 \pm j 2.99$	$-0.478 \pm j 3.14$
Dutch Roll Damping Ratio	0.12	0.15	0.15
Spiral Mode Roots	0.0121	0.0131	0.0139
Time to Double Amplitude	57.3 sec	52.9 sec	49.9 sec
Roll Convergence Roots	-6.49	-6.43	-6.18
Roll Mode Time Constant	0.154 sec	0.156 sec	0.162 sec
(b) Approach			
Dutch Roll Roots	$-0.243 \pm j 1.74$	$-0.321 \pm j 1.85$	$-0.371 \pm j 1.93$
Dutch Roll Damping Ratio	0.14	0.17	0.19
Spiral Mode Roots	0.0106	0.0143	0.0175
Time to Double Amplitude	65.4 sec	48.5 sec	39.6 sec
Roll Convergence Roots	-4.37	-4.32	-4.13
Roll Mode Time Constant	0.229 sec	0.231 sec	0.242 sec

Applying the criteria of reference 9 to the characteristics of table V, it appears that the fixed-trimmer configuration meets all of the Level I standards for all three fuselage deck angles and for both the cruise and approach flight conditions. Even though the spiral mode is divergent in all cases, the time to double amplitude is greater than the minimum of 20 seconds as specified in reference 9.

The calculations were repeated for wing sweep angles of 10 degrees and 20 degrees for the more sensitive approach configuration. Wing sweep angle was found to have little effect on the damping ratio of the dutch roll mode for either the free or fixed trimmers. The only significant effect was to stabilize the spiral mode for the 20-degree sweep, fixed-trimmer case.

For comparison purposes, calculations were also performed for an equivalent fixed-wing conventional aircraft, geometrically similar to the aircraft of figure 2, but with no external trimmers. These calculations are summarized in table VI.

TABLE VI. LATERAL-DIRECTIONAL CHARACTERISTICS
EQUIVALENT CONVENTIONAL AIRCRAFT

	Cruise	Approach
Dutch Roll Roots	$-0.596 \pm j 3.59$	$-0.451 \pm j 2.27$
Dutch Roll Damping Ratio	0.16	0.19
Spiral Mode Roots	0.00793	0.0564
Time to Double Amplitude	87.4 sec	12.3 sec
Roll Convergence Root	-6.58	-4.43
Roll Mode Time Constant	0.152 sec	0.226 sec

A comparison of the data in the tables indicates that the characteristics of the fixed aft trimmer are very similar to the conventional airplane, except for some reduction in dutch roll frequency because of greater roll and yaw inertias.

The free aft trimmer causes a reduction in dutch roll damping with negative fuselage trim attitudes, but tends to stabilize the spiral mode in all cases.

It is the effect of sideslip angle which is the primary cause of differences between the fixed and free aft trimmer characteristics. In sideslip, the trimmer on the advancing wing tends to float leading edge up, with an opposite effect on the leeward trimmer. This movement, in turn, creates a rolling moment away from the sideslip, thereby contributing to the total dihedral effect of the configuration.

Since the coefficient governing this motion, $C_{mR\beta}$, is relatively difficult to predict analytically with precision, as discussed in appendix C, its effect was examined parametrically. Fortunately, for the approach case with zero fuselage deck angle, it was found that it would be necessary to almost double the computed value of $C_{mR\beta}$ to create an instability of the dutch roll mode.

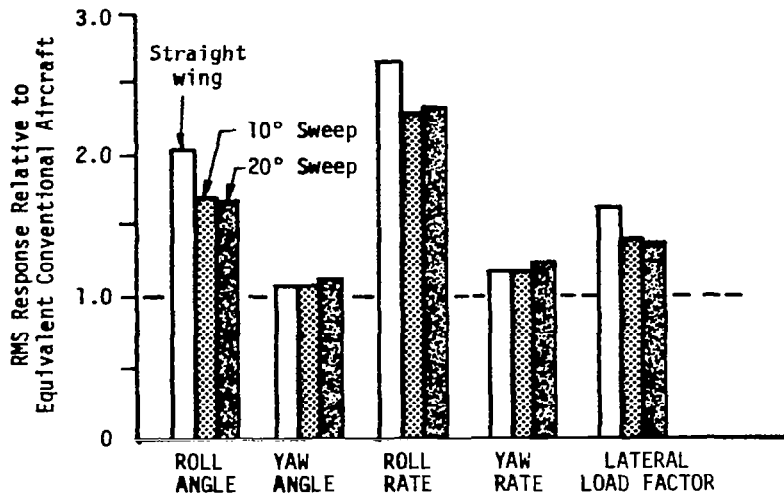
The lateral-directional responses to continuous atmospheric turbulence were determined by computing the combined effects of uncorrelated rolling and sideslip gusts of unit rms intensity (1 meter/second). The procedure is outlined in appendix D, and the results are listed in table VII. For the free and fixed trimmers, zero fuselage deck angle was assumed.

In most respects, the fixed trimmer turbulence response is the same or slightly better than the conventional airplane, except for slightly increased yaw angle response. The aft free-trimmer configuration, on the other hand, has a substantial increase in rolling response, especially in the approach configuration, where the rms roll angle is about twice that of the fixed-trimmer airplane or the conventional aircraft.

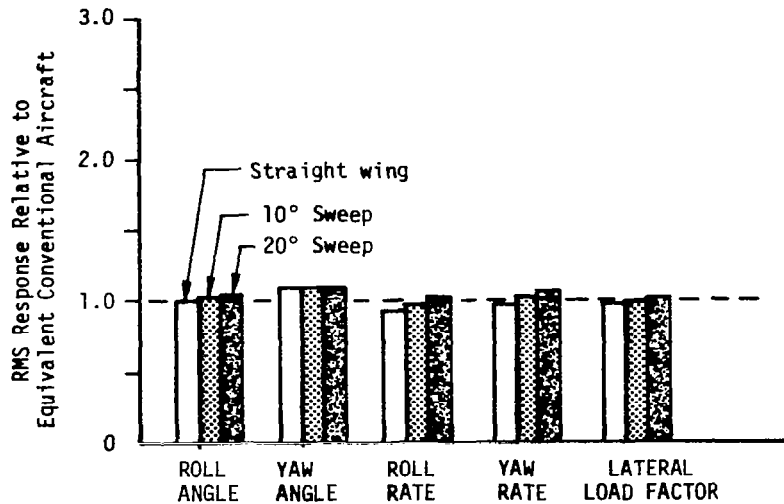
The turbulence responses relative to the conventional fixed-wing-equivalent airplane are depicted graphically in figure 14 for the three wing sweep angles. These calculations were made for the approach flight condition with zero fuselage deck angle.

Wing sweep angle is seen to have only a very small effect on the gust response characteristics.

As a final check on lateral-directional behavior, time histories were computed for step lateral control displacement. Again, the straight-wing aircraft of figure 2 was used with zero fuselage deck angle.



(a) Free Trimmer



(b) Fixed Trimmer

FIGURE 14. LATERAL DIRECTIONAL TURBULENCE RESPONSES OF AFT TRIMMER CONFIGURATIONS, APPROACH, ZERO FUSELAGE DECK ANGLE

TABLE VII. RMS LATERAL-DIRECTIONAL RESPONSES TO UNIT
TURBULENCE INTENSITY (ZERO SWEEP ANGLE,
ZERO FUSELAGE DECK ANGLE)

	Conventional Aircraft	Fixed Trimmer	Free Trimmer
(a) Cruise			
Roll Angle, Deg	1.122	1.106	1.270
Yaw Angle, Deg	0.793	0.853	0.827
Roll Rate, Deg/Sec	1.614	1.480	2.103
Yaw Rate, Deg/Sec	1.585	1.522	1.532
Lateral Path Displacement, Meters	0.973	0.968	0.991
Side Load Factor, g's	0.0244	0.0251	0.0231
(b) Approach			
Roll Angle, Deg	1.401	1.404	2.831
Yaw Angle, Deg	1.247	1.348	1.368
Roll Rate, Deg/Sec	1.634	1.503	4.331
Yaw Rate, Deg/Sec	1.526	1.499	1.775
Lateral Path Displacement, Meters	1.210	1.250	1.280
Side Load Factor, g's	0.0259	0.0258	0.0423

Figure 15 compares the cruise and approach histories for the free-trimmer configuration. In these cases, the disturbance is created by step differential displacement of the control tabs on the left and right trimmer surfaces, creating the trimmer responses shown in the lower traces.

An interesting feature of the free trimmer lateral control responses is the proverse "aileron" yaw which is exhibited at both the cruise and approach conditions. Whereas one might have expected considerable adverse yaw with equal differential displacement of the large outboard trimming surfaces, the opposite effect prevails because of the negative trim lift which exists on the trimmers. During an entry into a right roll, for example, the right trimmer is displaced (by action of its tab) in a leading-edge-down direction as shown in figure 15. This creates an increase in the negative trimmer lift with an associated increase in induced drag, creating a nose-right proverse yaw response. The effect is observed in the sideslip history, where the initial sideslip is negative. After the initial control-induced

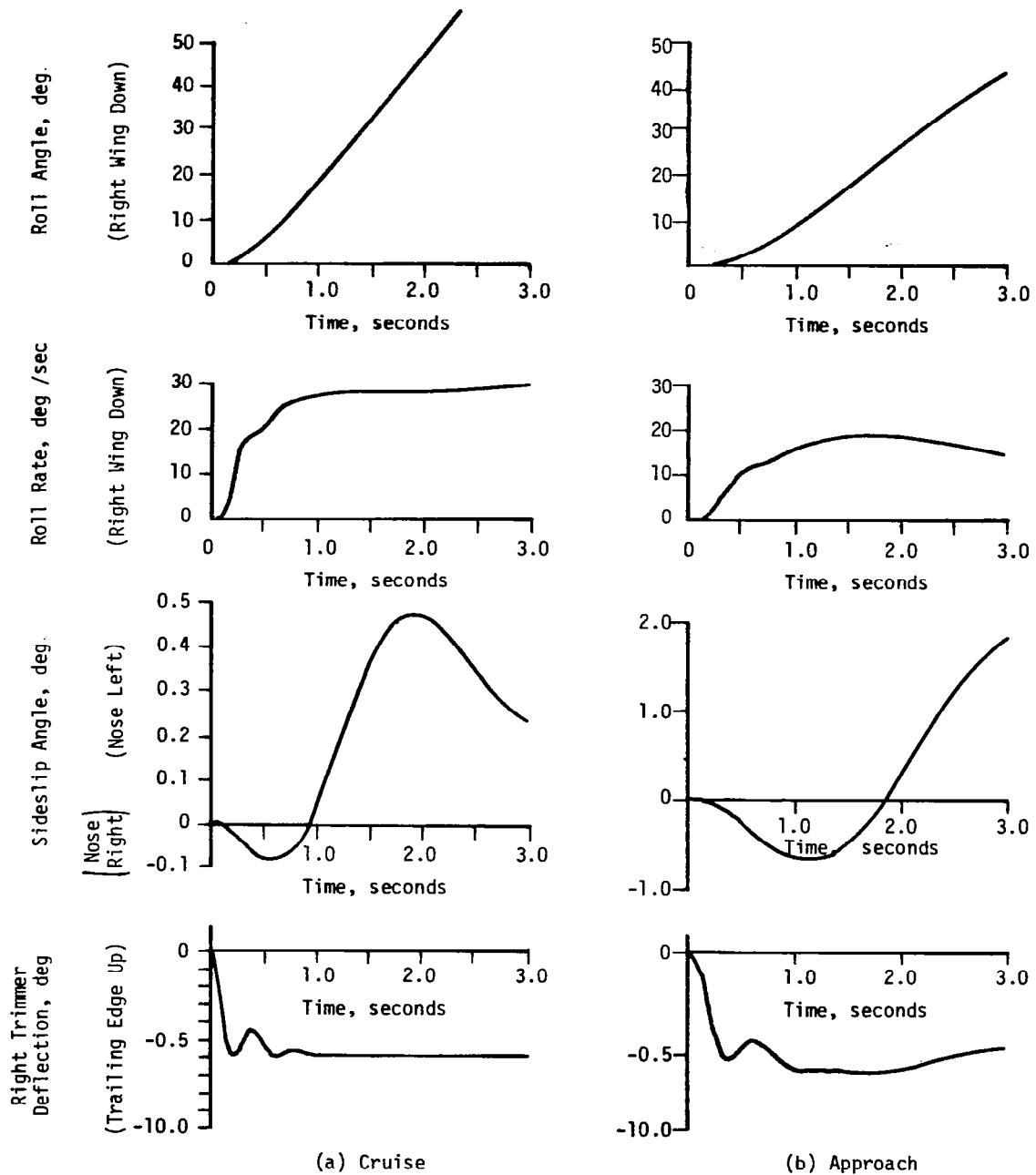


FIGURE 15. RESPONSES TO STEP LATERAL CONTROL INPUT, FREE TRIMMER CONFIGURATION

response, the sideslip changes sign because of the uncoordinated roll angle which has developed.

For the fixed-trimmer configuration (figure 16), the nature of the spanwise lift distribution depends upon whether or not the wing flaps are deflected. As noted previously (figure 9), the trimmer lift is positive for the no-flap condition, but becomes negative in the approach configuration to counter the wing flap pitching moment. This is in contrast to the free-trimmer arrangement, in which the trimmer lift is always negative in the equilibrium state.

Since the fixed-trimmer lift is positive in the cruise configuration, a leading-edge-down deflection of the trimmer on the downward-moving wing-tip will cause a reduction in trimmer-induced drag and an adverse yawing moment during roll entries.

The adverse yaw of the fixed trimmer for the cruise condition is apparent in the sideslip trace of figure 16(a), whereas proverse yaw effects are seen for the approach case in figure 16(b). In neither case is the sideslip transient sufficiently large to create a significant influence. The roll rate history is very nearly ideal in both cruise and approach.

Summary of Configuration Options

The results of this study, combined with the previous investigations cited as references, provide sufficient information to evaluate the potential of several variations of the basic free-wing principle. The generic concepts are:

- (1) Pure free wing with no external trimmer
- (2) Free wing/free forward trimmer
- (3) Free wing/free aft trimmer
- (4) Free wing/fixed aft trimmer.

The evidence indicates that each of these variants is feasible, within its respective limitations, to provide a stall-proof airplane which could be operated and maneuvered to the limits of its performance capability without fear of an inadvertent loss of control.

The selection of a particular variant is dependent on design objectives over and above stall-proof behavior. The selection would depend on the relative importance of high-lift capability, gust alleviation, and low structural weight. The relative advantages and disadvantages of each concept are summarized in table VIII.

With regard to the aggravated roll response of the aft fixed trimmer in turbulence, a simple, fail-safe, roll damper may be sufficient to

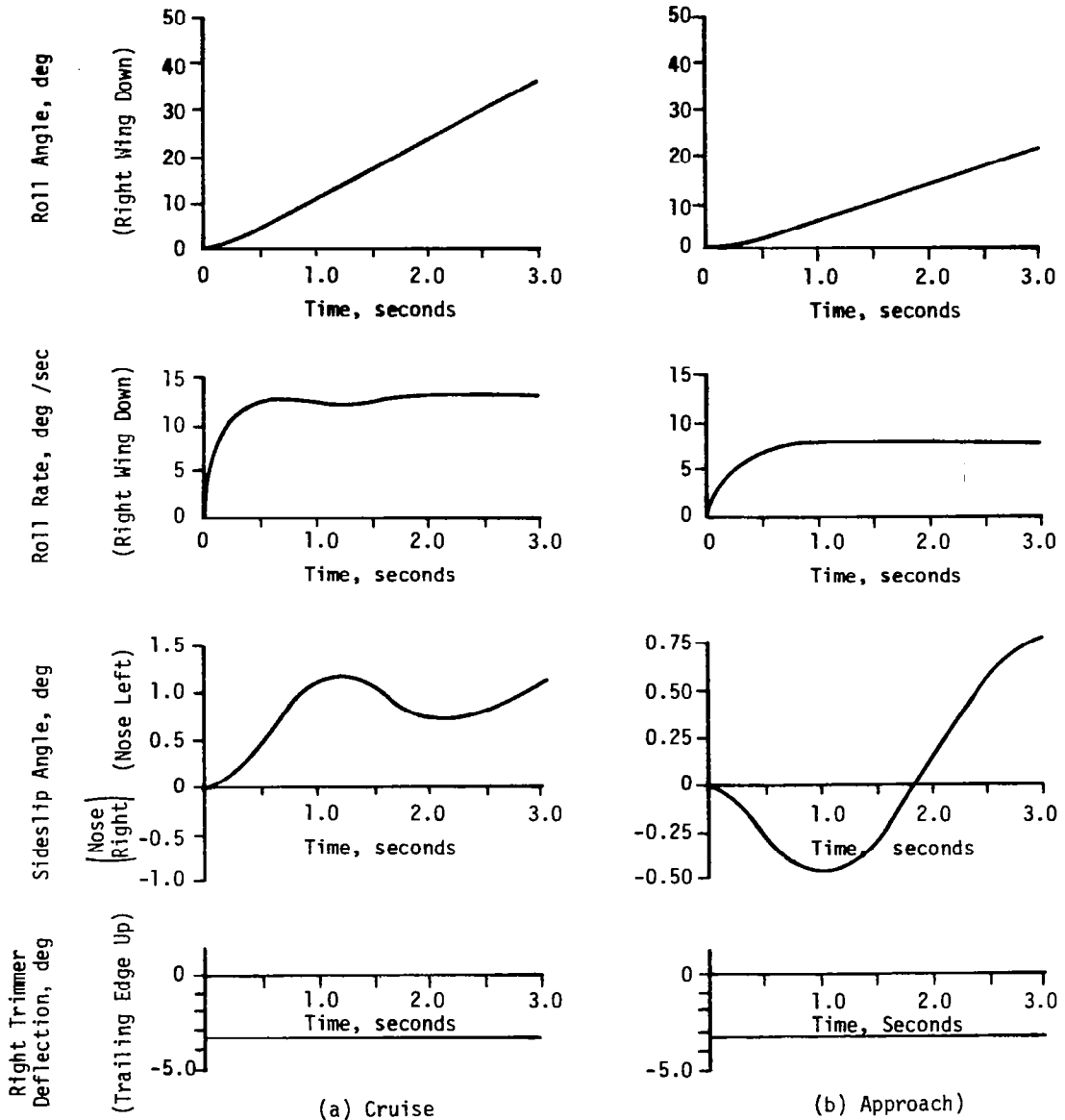


FIGURE 16. RESPONSES TO STEP LATERAL CONTROL INPUT, FIXED TRIMMER CONFIGURATION

reduce this effect. The roll damper was not evaluated in this study, however.

TABLE VIII. TRADE-OFF COMPARISON OF CONFIGURATIONS

Configuration	$C_{L_{MAX}}$	RMS Turbulence Response Compared to Fixed Wing		Increase in Empty Weight Compared to Fixed Wing ⁽²⁾	
		Normal Load Factor	Roll Angle		
Free Wing, No Trimmer	1.46 ⁽¹⁾	48%	Reduction	No Effect	7%
Forward Free Trimmer (figure 7)	1.75	15%	Reduction	Not Evaluated	8%
Aft Free Trimmer	1.75	53%	Reduction	100% Increase	27%
Aft Fixed Trimmer	2.12	30%	Reduction	No Effect	19%

(1) From Reference 3.

(2) Includes weight of trimmers, supporting booms, and counterweights required to balance the wing/trimmer assembly about the wing hinge axis.

CONCLUSIONS

From this investigation, the following conclusions are drawn:

(1) From a comparison of forward and aft-mounted free trimmers of equal trimmed lift capability, the forward trimmer is superior only with regard to structural weight. The forward trimmer concept has relatively little gust alleviation potential and exhibits a transient longitudinal control response characteristic which may be undesirable.

(2) The tip-mounted aft free-trimmer arrangement has excellent alleviation of the normal load factor response to vertical gusts, and good control response characteristics. Disadvantages are a high structural weight penalty and aggravated rolling motion in lateral-directional gust disturbances.

(3) If the aft tip trimmer is fixed but controllable by pilot input, the aerodynamic center of the wing/trimmer assembly moves aft and

permits a corresponding shift in wing hinge axis location. As a consequence, the weight penalty is reduced by 30 percent and the lift capability is sharply increased. Although there is some sacrifice in vertical gust alleviation, compared to the free-trimmer case, the control responses are good and there is no adverse effect on lateral-directional turbulence behavior. A disadvantage is the need for very effective high-lift devices on the fixed trimmer to preclude a catastrophic loss of control if the wing lift coefficient is inadvertently reduced to low values with flaps deflected.

(4) Differential trimmer movement can provide powerful and effective lateral control of both the free and fixed aft-trimmer configurations. The free trimmer exhibits proverse yaw characteristics, as does the fixed trimmer in the approach configuration. In the cruise configuration, the fixed trimmer induces some adverse yaw.

(5) The primary effect of fuselage trim attitude (deck angle) is on the damping ratio of the dutch roll mode. The tendency is for reduced damping at negative (nose-down) fuselage attitudes. The effect is most pronounced in the approach condition.

(6) Wing sweep angle, up to 20 degrees, had only a small effect on the dynamic behavior of any of the configurations examined. For structural reasons, a sweep angle of about 10 degrees appears optimum for the aft trimmer arrangements.

APPENDIX A. EQUATIONS OF MOTION

Introduction

The linearized equations of longitudinal motion of free-wing/free trimmer aircraft were developed in appendix B of reference 8. The only modification has been the addition of a pitch rate term in the wing pitching moment equation, arising from the consideration of swept wings.

The linear lateral-directional equations of motion were derived for free-wing aircraft with differential panel freedom in reference 2. For free-wing/free-trimmer aircraft with independent trimmers but wing panels constrained to symmetric pitching, the equations can be used directly. It is only necessary to redefine the free panel equation to represent the motion of the right trimmer rather than that of the right wing.

Both sets of equations are listed in this appendix.

Symbols

Longitudinal equations.

AR	wing aspect ratio
\bar{C}	mean aerodynamic wing chord, meters (feet)
\bar{C}_c	mean free trimmer chord, meters (feet)
C_{DF}	fuselage drag coefficient
$C_{D_{Oc}}, C_{D_{OW}}$	profile drag coefficients of free trimmer and wing, respectively
C_{Lc}, C_{LW}	lift coefficients of free trimmer and wing, respectively
$C_{L_{Oc}}, C_{L_{OW}}$	equilibrium lift coefficients of free trimmer and wing, respectively
$C_{L\alpha_c}, C_{L\alpha_W}, C_{L\alpha_F}$	lift-curve slopes per radian for free trimmer, wing, and fuselage, respectively, per radian
$C_{L\delta_t}$	$\partial C_L / \partial \delta_t$, per radian
C_m	pitching moment coefficient
$C_{m\alpha_F}$	$\partial C_m / \partial \alpha_F$, per radian

$C_{m\epsilon}$	$\partial C_m / \partial \epsilon$, per radian
C_{mq}	$\partial C_m / \partial \frac{q\bar{c}}{2U_0}$, per radian
$C_{m\delta_t}$	$\partial C_m / \partial \delta_t$, per radian
$\frac{dC_D}{dC_L^2}$	induced drag factor
E	ratio of wing semiperimeter to span
$F_{x_{c \rightarrow b}}$, $F_{z_{c \rightarrow b}}$	components of force transmitted from free trimmer to wing boom, newtons (pounds)
$F_{x_{w \rightarrow f}}$, $F_{z_{w \rightarrow f}}$	components of force transmitted from wing to fuselage, newtons (pounds)
g	acceleration of gravity, meters/second ² (feet/second ²)
G_{1c} , G_{1w}	transfer functions relating lift coefficient to angle of attack for free trimmer and wing, respectively
G_{2c} , G_{2w}	transfer functions relating lift coefficient to gust velocity for free trimmer and wing, respectively
I_{y_f}	pitching moment of inertia of fuselage assembly about wing hinge axis, kilogram-meters ² (slug-feet ²)
I_y'	pitching moment of inertia of wing/boom assembly about wing hinge axis, kilogram-meters ² (slug-feet ²)
I_y''	pitching moment of inertia of each free trimmer about its hinge axis, kilogram-meters ² (slug-feet ²)
l_c	distance from quarter chord of wing to quarter chord of free trimmer, measured positive forward, meters (feet)
l_t	distance from quarter chord of wing to quarter chord of fuselage mounted horizontal tail, measured positive rearward, meters (feet)
m_c , m_{WB} , m_F	mass of free trimmer, wing/boom assembly, and fuselage assembly, respectively, kilograms (slugs)
q	pitch rate of fuselage, radians/second
S	wing reference area, meters ² (feet ²)

S_C	free trimmer reference area, meters ² (feet ²)
U	true airspeed, meters/second (feet/second)
u	increment in airspeed divided by equilibrium airspeed
V_g	gust velocity, positive upward, meters/second (feet/second)
W	component of velocity along z_h -axis, meters/second (feet/second)
X_{ac}	distance from leading edge to aerodynamic center of wing, meters (feet)
X_F	distance from wing hinge forward to fuselage center of gravity, meters (feet)
\hat{X}_c, \hat{X}	distance from hinge point to one-half chord point for free trimmer and wing, respectively, meters (feet)
X'_{CH}	x' -coordinate of trimmer hinge axis relative to wing hinge, meters (feet)
X'_{cg}	x' -coordinate of center of gravity of wing/boom, relative to wing hinge, meters (feet)
X''_{cg}	distance of free-trimmer center of gravity forward of hinge line, meters (feet)
Z_F	z_h -component of displacement of fuselage center of gravity with respect to wing hinge, meters (feet)
Z'_{CH}	z' -coordinate of trimmer hinge axis relative to wing hinge, meters (feet)
Z'_{cg}	z' -coordinate of center of gravity of wing/boom, relative to wing hinge, meters (feet)
$\alpha_c, \alpha_F, \alpha_W$	angle of attack of free trimmer, fuselage, and wing, respectively, radians
δ_c	displacement of free trimmer with respect to wing, positive leading edge up, radians
δ_{c_0}	equilibrium value of δ_c , radians
δ_p	displacement of wing with respect to fuselage, positive leading edge up, radians
δ_{p_0}	equilibrium value of δ_p , radians

δ_t	displacement of control tab on free trimmer, positive trailing edge down, radians
ϵ	downwash angle, radians
θ	pitch angle of longitudinal fuselage axis with respect to horizon, radians
Λ	wing sweep angle, radians
λ	Laplace operator, per second
ρ	atmospheric density, kilograms/meter ³ (slugs/foot ³)
$\rho_{x_{cg}}, \rho_{z_{cg}}$	coordinates of wing boom center of gravity in wing hinge axis system, meters (feet)

Lateral-directional equations.

b	wing span, meters (feet)
\bar{c}	mean aerodynamic chord length, meters (feet)
C_ℓ	rolling-moment coefficient, positive for right roll
C_{ℓ_p}	$\partial C_\ell / \partial \left(\frac{pb}{2U_o} \right)$, per radian
$C_{\ell_{p_w}}$	wing contribution to C_{ℓ_p}
C_{ℓ_r}	$\partial C_\ell / \partial \left(\frac{rb}{2U_o} \right)$, per radian
C_{ℓ_β}	$\partial C_\ell / \partial \beta$, per radian
$C_{\ell_{\delta_{tR}}}$	$\partial C_\ell / \partial \delta_{tR}$, per radian
$C_{\ell_{\delta_c}}$	$\partial C_\ell / \partial \delta_c$, per radian
C_n	yawing-moment coefficient, positive nose right
C_{n_p}	$\partial C_n / \partial \left(\frac{pb}{2U_o} \right)$, per radian
C_{n_r}	$\partial C_n / \partial \frac{rb}{2U_o}$, per radian
C_{n_β}	$\partial C_n / \partial \beta$, per radian

$C_n \delta_c$	$\partial C_n / \partial \delta_c$, per radian
$C_n \delta_{t_R}$	$\partial C_n / \partial \delta_{t_R}$, per radian
C_y	side-force coefficient, positive to right
C_{y_p}	$\partial C_y / \partial \left(\frac{pb}{2U_o} \right)$, per radian
C_{y_r}	$\partial C_y / \partial \left(\frac{rb}{2U_o} \right)$, per radian
C_{y_β}	$\partial C_y / \partial \beta$, per radian
C_{y_δ}	$\partial C_y / \partial \delta_c$, per radian
D_y	lateral path displacement, positive to right, meters (feet)
I_y''	moment of inertia of each trimmer about hinge axis, kilogram-meters ²
I_{XX_T} , I_{ZZ_T}	moments of inertia of total aircraft, measured in the stability of axis system, kilogram-meters ² (slug-feet ²)
I_{XZ_T}	product of inertia of total aircraft, measured in the stability of axis system, kilogram-meters ² (slug-feet ²)
I_{XY_c} , I_{YZ_c}	products of inertia of trimmer, kilogram-meters ² (slug-feet ²)
L_p	$\frac{\rho U_o S b^2}{4 I_{XX_T}} C_{\ell_p}$
L_{p_w}	$\frac{\rho U_o S B^2}{4 I_{XX_T}} C_{\ell_{p_w}}$
L_r	$\frac{\rho U_o S b^2}{4 I_{XX_T}} C_{\ell_r}$
L_β	$\frac{\rho U_o^2 S b}{2 I_{XX_T}} C_{\ell_\beta}$

m	total mass of aircraft, kilograms (slugs)
M_{RP}	$\frac{\rho U_o S \bar{c} b}{4 I_{y''}} C_{mRP}$
M_{Rr}	$\frac{\rho U_o S \bar{c} b}{4 I_{y''}} C_{mRr}$
$M_{R\beta}$	$\frac{\rho U_o^2 S \bar{c}}{2 I_{y''}} C_m$
N_p	$\frac{\rho U_o S b^2}{4 I_{ZZT}} C_{np}$
N_{pw}	$\frac{\rho U_o S b^2}{4 I_{ZZT}} C_{npw}$
N_r	$\frac{\rho U_o S b^2}{4 I_{ZZT}} C_{nr}$
N_β	$\frac{\rho U_o^2 S b}{2 I_{ZZT}} C_{n\beta}$
p	roll rate about X_s stability axis, radians/second
r	yawing rate about Z_s stability axis, radians/second
S	total wing area, meters ² (feet ²)
U_o	equilibrium velocity of aircraft center of gravity along X stability axis, meters/second (feet/second)
Y_p	$\frac{\rho S b}{4 m} C_{yp}$
Y_r	$\frac{\rho S b}{4 m} C_{yr}$

Y_{β}	$\frac{\rho U_o S}{2m} C_{y_{\beta}}$
β	sideslip angle, positive with wind from right, radians
β_g	apparent sideslip caused by lateral gust, radians
δ_{cR}	displacement of right trimmer with respect to wing, positive trailing edge down, radians
δ_{tR}	displacement of control tab on right trimmer, positive trailing edge down, radians
λ	Laplace operator, per second
ϕ	roll angle, positive right wing down, radians
ϕ_g	apparent rolling gust created by spanwise gradient of vertical gust velocity, radians/second
ρ	atmospheric density, kilograms/meter ³ (slugs/feet ³)
ψ	yaw angle, positive nose right, radians

Coordinate Systems

The longitudinal and lateral-directional equations employ separate coordinate axis systems. These axis systems are shown in figure 17.

The longitudinal equations are written with respect to a wing hinge axis system. The origin is at the intersection of the wing hinge axis and the plane of lateral symmetry of the aircraft. The x_h axis is positive forward in the direction of flight in the equilibrium condition. The y_h axis is positive toward the right wing. The z_h axis completes the right-handed set, positive downward.

The lateral-directional equations are written with respect to a conventional stability axis system with origin at the center of gravity of the complete aircraft. The x_s axis is aligned with the velocity vector of the aircraft in the reference condition, the y_s axis extends to the right of the plane of symmetry, and the z_s axis completes the right-hand set. These coordinates are fixed to the aircraft and rotate with it.

The orientation of the stability axis system with respect to an inertially fixed reference is defined by three standard Euler angles. The sequence of rotation used to define these angles is (1) rotation about the z axis through the yaw angle ψ , (2) rotation about the y axis through the pitch angle, θ , and (3) rotation about the x axis through the roll angle ϕ .

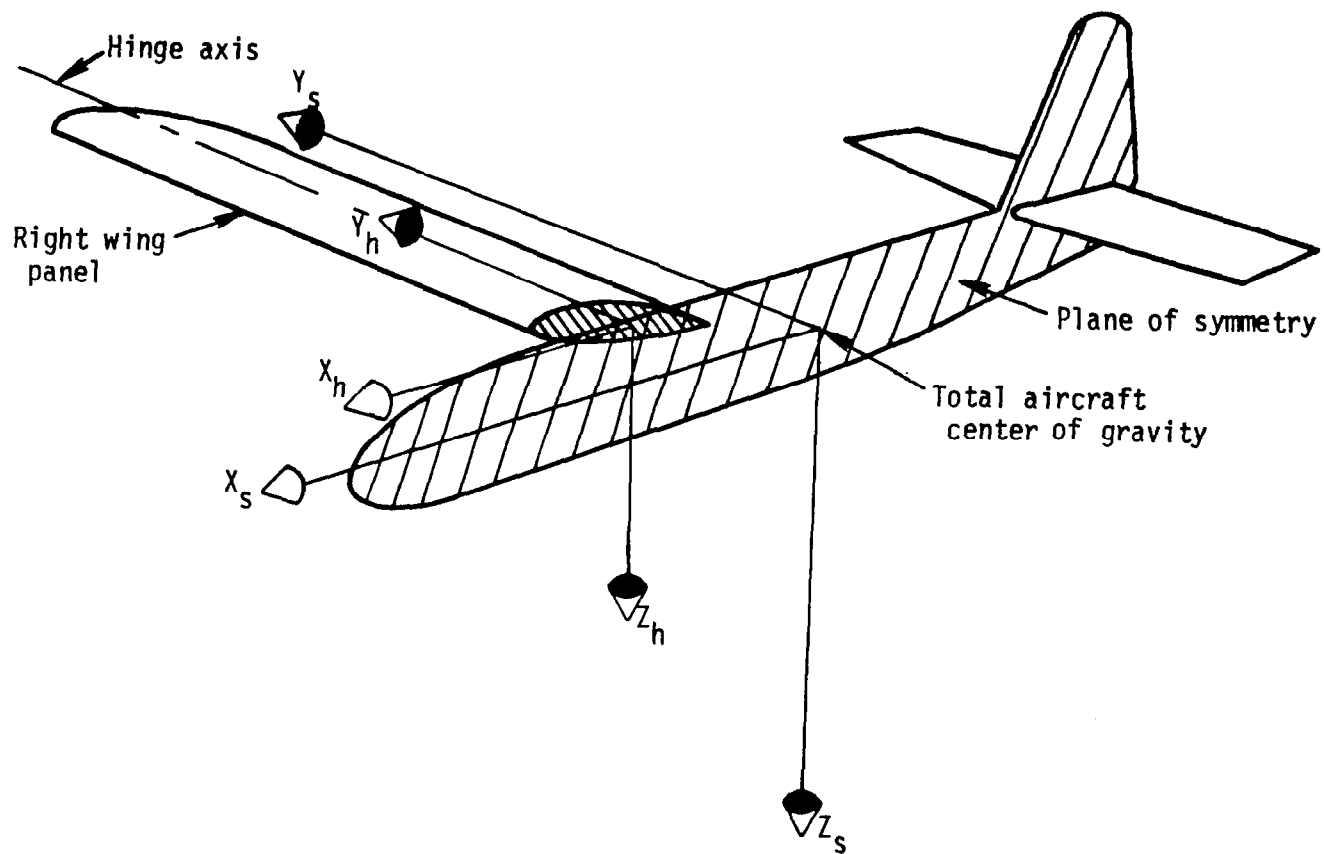


FIGURE 17. ILLUSTRATION OF AXIS SYSTEMS

Longitudinal Equations

The longitudinal system is composed of three rigid bodies coupled together by geometric and kinematic constraints. The three bodies are the free-trimmer panel, the wing/boom assembly, and the fuselage assembly.

Force and moment equations were developed for each free body in linearized form with motion confined to the vertical plane. Although these individual equations implicitly contain the geometric and kinematic constraints, the forces transmitted through the trimmer hinge and the wing hinge are treated as separate, dependent variables. Furthermore, because of the complexity of the representation of unsteady aerodynamic forces (see appendix B), it is also convenient to treat the circulatory lift coefficients of the wing and trimmer surfaces as additional explicit variables.

As employed in this study, the equations represent a departure from conventional analysis. Although the number of dependent equations could have been reduced, and all of the forces and moments could have been referred to the total aircraft center of gravity, as is customary, the physical significance and origins of the individual terms in the equations would have become obscure. In short, the individual equations are retained as they were derived to facilitate their verification - not a trivial consideration for such a complex system.

The longitudinal equations are written with respect to the wing hinge axis system shown in figure 17.

The set of equations is listed below in operational form.

Trimmer angle of attack.

$$[-1]\alpha_c + [1]\alpha_f + [1 + (C1)\lambda]\delta_p + [1 + (C3)\lambda]\delta_c + [(C2)\lambda]\theta + [C4]C_{LW} = 0 \quad (3)$$

$$C1 = C2 = - \frac{X'_{CH} \cos \delta_{p_o} + Z'_{CH} \sin \delta_{p_o} + \hat{X}_c \cos(\delta_{p_o} + \delta_{c_o})}{U_o} \quad (4)$$

$$C3 = - \frac{\hat{X}_c}{U_o} \cos(\delta_{p_o} + \delta_{c_o}) \quad (5)$$

$$C4 = \frac{d\alpha_c}{dC_{LW}} \quad (6)$$

Trimmer lift coefficient.

$$\begin{aligned}
 & \left[-\left(\lambda + 0.598 \frac{U_o}{\bar{C}_c} \right) \right] C_{L_c} + \left[0.639 C_{L_{\alpha_c}} \lambda + 0.598 \frac{U_o}{\bar{C}_c} C_{L_{\alpha_c}} \right] \alpha_c \\
 & + \left[C_{L_{\alpha_c}} (C5) \left(0.639 \lambda^2 + 0.598 \frac{U_o}{\bar{C}_c} \lambda \right) \right] \delta_p + \left[C_{L_{\alpha_c}} (C5) \left(0.639 \lambda^2 \right. \right. \\
 & \left. \left. + 0.598 \frac{U_o}{\bar{C}_c} \lambda \right) \right] \theta + \left[C_{L_{\alpha_c}} (C5) \left(0.639 \lambda^2 + 0.598 \frac{U_o}{\bar{C}_c} \right) \right] \delta_c \quad (7) \\
 = & - \left[C_{L_{\alpha_c}} (C6) \left(0.639 \lambda + 0.598 \frac{U_o}{\bar{C}_c} \right) \right] \delta_t - \left[G_{2c} \left(\lambda + 0.598 \frac{U_o}{\bar{C}_c} \right) \left(\frac{l_{c\lambda}}{U_o} + 1 \right) \right] \frac{v_g}{U_o}
 \end{aligned}$$

where

$$C5 = \frac{\bar{C}_c}{\pi U_o} \quad (8)$$

$$C6 = \frac{C_{L_{\alpha_c}} \delta_t}{C_{L_{\alpha_c}}} \quad (9)$$

$$G_{2c} = C_{L_{\alpha_c}} \left[1 - \frac{0.488 \lambda}{\lambda + 0.455 \frac{U_o}{\bar{C}_c}} - \frac{0.272 \lambda}{\lambda + 1.04 \frac{U_o}{\bar{C}_c}} - \frac{0.193 \lambda}{\lambda + 4.71 \frac{U_o}{\bar{C}_c}} \right] \quad (10)$$

Trimmer pitching moment equation.

$$\begin{aligned}
 & [(C22) \lambda^2 + (C30 - C31) \lambda] \delta_c + [-(C30) \lambda] \alpha_c + [-C29] C_{L_c} \\
 & + [(C27) \lambda] \alpha_p + [(C23) \lambda^2 + (C30 - C31) \lambda] \alpha_p + [(C24) \lambda^2 + \\
 & (C25 - C31) \lambda] \theta + [(C26) \lambda] u = +[C28] \delta_t \quad (11)
 \end{aligned}$$

where

$$C22 = I_{y''} \quad (12)$$

$$C23 = I_{y''} + m_c \rho_{z_{H_c}} \left(Z'_{CH} \cos \delta_{P_o} - X'_{CH} \sin \delta_{P_o} \right) \quad (13)$$

$$+ m_c \rho_{x_{H_c}} \left(Z'_{CH} \sin \delta_{P_o} = X'_{CH} \cos \delta_{P_o} \right)$$

$$C24 = C23 \quad (14)$$

$$C25 = m_c \rho_{x_{H_c}} U_o \quad (15)$$

$$C26 = m_c \rho_{z_{H_c}} U_o \quad (16)$$

$$C27 = -C25 \quad (17)$$

$$C28 = C_{m_{\delta_t}} 1/2 \rho U_o^2 S_c \bar{c}_c \quad (18)$$

$$C29 = 1/2 \rho U_o^2 S_c \left(\hat{X}_c + \frac{\bar{c}_c}{4} \right) \quad (19)$$

$$C30 = \frac{\rho U_o S_c \bar{c}_c}{E} \hat{X}_c \quad (20)$$

$$C31 = \frac{\rho U_o S_c \bar{c}_c}{E} \left(\hat{X}_c - \frac{\bar{c}_c}{4} \right) \quad (21)$$

$$\rho_{x_{H_c}} = X''_{cg} \cos \left(\delta_{P_o} + \delta_{c_o} \right) \quad (22)$$

$$\rho_{z_{H_c}} = -X''_{cg} \sin \left(\delta_{P_o} + \delta_{c_o} \right) \quad (23)$$

Longitudinal components of trimmer hinge force.

$$\begin{aligned}
 & [-1]F_{x_{c \rightarrow b}} + [C12]C_{L_c} + [(C9 + C10)\lambda^2]\delta_p + [C13 + (C9 + C10)\lambda^2]\phi \\
 & + [(C10)\lambda^2]\delta_c + [C11 + (C7)\lambda]u = 0
 \end{aligned} \tag{24}$$

where

$$C7 = -m_c U_o \tag{25}$$

$$C9 = -m_c \left(Z'_{CH} \cos \delta_{p_o} - X'_{CH} \sin \delta_{p_o} \right) \tag{26}$$

$$C10 = -m_c \left[-X''_{cg} \sin (\delta_{p_o} + \delta_{c_o}) + Z''_{cg} \cos (\delta_{p_o} + \delta_{c_o}) \right] \tag{27}$$

$$C11 = - \left[C_{D_{o_c}} + \frac{dC_D}{dC_L^2} C_{L_{o_c}}^2 \right] \rho U_o^2 S_c \tag{28}$$

$$C12 = - \frac{dC_D}{dC_L^2} C_{L_{o_c}} \rho U_o^2 S_c \tag{29}$$

$$C13 = -m_c g \tag{30}$$

Normal component of trimmer hinge force.

$$\begin{aligned}
 & [-1]F_{z_{c \rightarrow b}} + [(C14)\lambda]\alpha_F + [(C15)\lambda + (C17 + C18)\lambda^2]\theta \\
 & + [(C17 + C18)\lambda^2]\delta_p + [(C18)\lambda^2]\delta_c + [C19]C_{L_c} \\
 & + [(C20)\lambda]\alpha_c + [C21]u = 0
 \end{aligned} \tag{31}$$

where

$$C14 = -m_c U_o \tag{32}$$

$$C15 = -C14 \quad (33)$$

$$C17 = m_c \left\{ Z'_{CH} \sin \delta_{p_o} + X'_{CH} \cos \delta_{p_o} \right\} \quad (34)$$

$$C18 = m_c \left[X''_{CG} \cos \left(\delta_{p_o} + \delta_{c_o} \right) \right] \quad (35)$$

$$C19 = -1/2 \rho U_o^2 S_c \quad (36)$$

$$C20 = - \frac{\rho U_o S_c \bar{c}_c}{E} \quad (37)$$

$$C21 = -C_{L_{o_c}} \rho U_o^2 S_c \quad (38)$$

Wing angle of attack.

$$[-1]\alpha_W + [1]\alpha_F + [1 + (C33)\lambda]\delta_p + [(C33)\lambda]\theta + [C34]C_{L_c} = 0 \quad (39)$$

where

$$C33 = - \frac{\hat{X}}{U} \cos \delta_{p_o} \quad (40)$$

$$C34 = \frac{d\alpha_W}{dC_{L_c}} \quad (41)$$

Wing lift coefficient.

$$\begin{aligned} & - \left[\lambda + 0.598 \frac{U_o}{\bar{c}} \right] C_{L_W} + \left[C_{L_{\alpha_W}} \left(0.639\lambda + 0.598 \frac{U_o}{\bar{c}} \right) \right] \alpha_w \\ + & \left[C36 C_{L_{\alpha_W}} \lambda \left(0.639\lambda + 0.598 \frac{U_o}{\bar{c}} \right) \right] \delta_p + \left[C36 C_{L_{\alpha_W}} \left(0.639\lambda \right. \right. \\ & \left. \left. + 0.598 \frac{U_o}{\bar{c}} \right) \right] \theta = \left[- \left(\lambda + 0.598 \frac{U_o}{\bar{c}} \right) G_{2W} \right] \frac{v_g}{U_o} \end{aligned} \quad (42)$$

$$C36 = \frac{\hat{X}}{U_o} \left(.25 - \frac{\hat{X}}{C} \right) \quad (43)$$

$$G_{2W} = C_{I\alpha W} \left[1 - \frac{0.488 \lambda}{\lambda + 0.455 \frac{U_o}{\bar{C}}} - \frac{0.272 \lambda}{\lambda + 1.04 \frac{U_o}{\bar{C}}} - \frac{0.193 \lambda}{\lambda + 4.71 \frac{U_o}{\bar{C}}} \right] \quad (44)$$

It may be noted that the equation for constant C36 differs from the expression given in reference 8. This is consistent with a modified approach to the inclusion of unsteady aerodynamic effects, as discussed in appendix B.

Longitudinal component of wing hinge force.

$$\begin{aligned} & [-1]F_{x_w \rightarrow f} + [C38 + (C40)\lambda]u + [C39]C_{LW} + [1]F_{x_c \rightarrow b} \\ & + [C43 + (C42)\lambda^2]\theta + [(C42)\lambda^2]\delta_p = 0 \end{aligned} \quad (45)$$

where

$$C38 = - \left(C_{D_{oW}} + \frac{dC_D}{dC_{LW}^2} C_{L_{oW}}^2 \right) \rho U_o^2 S \quad (46)$$

$$C39 = - \frac{dC_D}{dC_{LW}^2} C_{L_{oW}} \rho U_o^2 S \quad (47)$$

$$C40 = -m_{WB} U_o \quad (48)$$

$$C42 = -m_{WB} \left(-X'_{cg} \sin \delta_{P_o} + Z'_{cg} \cos \delta_{P_o} \right) \quad (49)$$

$$C43 = -m_{WB} g \quad (50)$$

Normal component of wing hinge force.

$$\begin{aligned}
 & [-1]F_{z_{w \rightarrow f}} + [C44]C_{L_W} + [(C45)\lambda]\alpha_W + [C46]u \\
 & + [1]F_{z_{c \rightarrow b}} + [(C47)\lambda]\alpha_F + [(-C47)\lambda + (C49)\lambda^2]\theta \\
 & + [(C49)\lambda^2]\delta_p = 0
 \end{aligned} \tag{51}$$

$$C44 = -1/2 \rho U_o^2 S \tag{52}$$

$$C45 = - \frac{\rho U_o \bar{S} C}{E} \tag{53}$$

$$C46 = -C_{L_{O_W}} \rho U_o^2 S \tag{54}$$

$$C47 = C40 \tag{55}$$

$$C49 = m_{WB} \left(X'_{cg} \cos \delta_{p_o} + Z'_{cg} \sin \delta_{p_o} \right) \tag{56}$$

Wing pitching moment equation.

$$\begin{aligned}
 & [C51 + (C56 - C55)\lambda + (C50)\lambda^2]\delta_p + [C51 + (C560 + C56 + C52)\lambda + (C50)\lambda^2]\theta \\
 & + [(C53)\lambda]u + [C54]C_{L_W} + [-(C52)\lambda]\alpha_F + [(C55)\lambda]\alpha_W \\
 & + [C57]F_{x_{c \rightarrow b}} + [C58]F_{z_{c \rightarrow b}} = 0
 \end{aligned} \tag{57}$$

where

$$C50 = I_{y'} \tag{58}$$

$$C51 = m_{WB} g Z'_{cg} \quad (59)$$

$$C52 = m_{WB} \rho_{x_{cg}} U_o \quad (60)$$

$$C53 = m_{WB} \rho_{z_{cg}} U_o \quad (61)$$

$$C54 = -1/2 \rho U_o^2 S \left(\hat{X} + \frac{\bar{C}}{2} - \frac{X_{ac}}{\bar{C}} \bar{C} \right) \quad (62)$$

$$C55 = - \frac{\rho U_o S \bar{C}}{E} \hat{X} \quad (63)$$

$$C56 = - \frac{\rho U_o S \bar{C}}{E} \left(\hat{X} - \frac{\bar{C}}{4} \right) \quad (64)$$

$$C560 = C_{L\alpha_W} \rho U_o S \bar{C}^2 (AR)^2 \tan^2 \Lambda / 96. \quad (65)$$

$$C57 = X'_{CH} \sin \delta_{p_o} - Z'_{CH} \cos \delta_{p_o} \quad (66)$$

$$C58 = X'_{CH} \cos \delta_{p_o} + Z'_{CH} \sin \delta_{p_o} \quad (67)$$

Equation 57 corresponds to equation 146 of reference 8, where it was printed incorrectly. In addition, the constant C560 has been added to allow for wing sweep as discussed in appendix B.

Fuselage pitching moment equation.

$$[C62 + (C65 - C61)\lambda - (C59)\lambda^2]\theta + [(C60)\lambda]u + [C63 + (C61)\lambda]\alpha_F \quad (68)$$

$$+ [C66]C_{L_W} + \{[C63] + [(C64)(C63) - C65]\lambda\} \frac{v}{U_o} = 0$$

where

$$C59 = I_{y_f} \quad (69)$$

$$C60 = -m_F Z_F U_o \quad (70)$$

$$C61 = m_F X_F U_o \quad (71)$$

$$C62 = -m_F g Z_F \quad (72)$$

$$C63 = 1/2 \rho U_o^2 S \bar{C} C_{m_{\alpha F}} \quad (73)$$

$$C64 = -\frac{l_t}{U_o} \quad (74)$$

$$C65 = 1/4 \rho U_o S (\bar{C})^2 C_{m_q} \quad (75)$$

$$C66 = \left(C_m \frac{1}{\epsilon} \right) \left(\frac{1}{2} \rho U_o^2 S \bar{C} \right) \left(\frac{\frac{d\epsilon}{d\alpha}}{C_{L_{\alpha W}}} \right) \quad (76)$$

Airspeed.

$$[C69 - (C67)\lambda]u + [C70 + (C68)\lambda^2]\theta + [1]F_{x_{w \rightarrow f}} = 0 \quad (77)$$

where

$$C67 = m_F U_o \quad (78)$$

$$C68 = -m_F Z_F \quad (79)$$

$$C69 = -C_{D_F} \rho U_o^2 S \quad (80)$$

$$C70 = -m_F g \quad (81)$$

Fuselage angle of attack.

$$\begin{aligned} [C72 - (C67)\lambda]\alpha_F + [(C67)\lambda + (C71)\lambda^2]\theta + [1]_{Fz}^{w \rightarrow f} \\ + [C73]u = -[C72] \frac{V}{U_o} \end{aligned} \quad (82)$$

where

$$C67 = m_F U_o \quad (83)$$

$$C71 = m_F X_F \quad (84)$$

$$C72 = -C_{L\alpha_F} \frac{\rho U_o S}{2} \quad (85)$$

$$C73 = -C_{L_{F_o}} \rho U_o^2 S \quad (86)$$

Lateral-Directional Equations

The lateral-directional equations are linearized about straight and level flight and are written with respect to a conventional stability axis system as shown in figure 17.

Unsteady aerodynamic effects are not explicitly included in the lateral-directional equations because the natural frequency of the free-panel motion is much higher than the rigid-aircraft lateral directional characteristic modes.

It is necessary to model the pitching motion of right free panel only. A separate equation for the left panel is not required since it can be shown to be equal in magnitude but opposite in sign to the right panel deflection for small perturbations in the lateral-directional variables.

The equations, as used to model the aircraft with free trimmers, are listed below in operational form.

Rolling moment equation.

$$\begin{aligned} \left(-\lambda^2 + L_p \lambda \right) \theta + \left(\frac{I_{XX_T}}{I_{XX_T}} \lambda^2 + L_r \lambda \right) \psi + L_\beta \beta + 2 \left(\frac{I_{XY_c}}{I_{XX_T}} \lambda^2 + L_{\delta_c} \right) \delta_{c_R} \\ = -2 L_{\delta_{t_r}} \delta_{t_r} - L_{p_w} \dot{\phi}_g - L_\beta \beta_g \end{aligned} \quad (87)$$

Yawing moment equation.

$$\begin{aligned} \left(\frac{I_{XZ_T}}{I_{ZZ_T}} \lambda^2 + N_p \lambda \right) \phi + \left(-\lambda^2 + N_r \lambda \right) \psi + N_\beta \beta + 2 \left(\frac{I_{YZ_c}}{I_{ZZ_T}} \lambda^2 + N_{\delta_c} \right) \delta_{c_R} \\ = -2 N_{\delta_{t_r}} \delta_{t_r} - N_{p_w} \dot{\phi}_g - \left(N_\beta + N_r \lambda \right) \beta_g \end{aligned} \quad (88)$$

Side force equation.

$$\left(Y_p \lambda + \frac{g}{U_o} \right) \phi + \left(Y_r - 1 \right) \lambda \psi + \left(-\lambda + Y_\beta \right) \beta + 2 Y_{\delta_c} \delta_{c_R} = -Y_\beta \beta_g \quad (89)$$

Right trimmer hinge moment equation.

$$\begin{aligned} \left(\frac{I_{XY_c}}{I_{y''}} \lambda^2 + M_{R_p} \right) \phi + \left(\frac{I_{YZ_c}}{I_{y''}} \lambda^2 + M_{R_r} \lambda \right) \psi + M_{R_\beta} \beta \\ + \left(-\lambda^2 + M_{R_\delta} \lambda + M_{R_{\delta_c}} \right) \delta_{c_R} = -M_{R_{\delta_{t_r}}} \delta_{t_r} - M_{R_p} \dot{\phi}_g - M_{R_\beta} \beta_g \end{aligned} \quad (90)$$

Lateral path displacement equation.

$$\lambda D_y = U_o (\psi + \beta) \quad (91)$$

APPENDIX B. LINEAR APPROXIMATION OF UNSTEADY AERODYNAMIC EFFECTS

References 2 and 4 have established the necessity of including unsteady aerodynamic effects for free wings for longitudinal analyses. Unless unsteady aerodynamics are considered, predictions of wing pitching frequency and gust alleviation can be too optimistic.

The analysis technique employed in this study required a linear approximation, in the form of a transfer function, to the circulatory lift response to angle-of-attack changes, as well as the noncirculatory contributions arising from apparent mass effects.

In references 2, 3, and 8, only straight wings were considered, and the approach to unsteady aerodynamic modeling followed the results given in reference 10 for an elliptical wing of aspect ratio 6. In particular, the transfer-function approximation to Theodorsen's function was obtained by taking the Laplace transform of the time derivative of the indicial response approximation of reference 10.

For the current study, swept wing planforms were to be considered, and appropriate indicial response functions could not be found. To fill this void, the required indicial responses were computed by the approach outlined in the following paragraphs.

The first step was to duplicate the indicial response function, given by Jones in reference 10, for a two-dimensional wing section. A modified lifting-line technique was used with a single bound vortex at the quarter-chord point and a control point located at the three-quarter-chord position, where the induced flow from the bound vortex equals the free-stream velocity normal to the surface for steady-state two-dimensional flow.

At the beginning of the motion, it is known that the bound circulation, which must be equal and opposite to the initial shed starting vortex, is one-half the final value. Satisfying this condition, as well as the boundary condition at the control point, required placement of the initial shed vortex one quarter chord aft of the trailing edge. Then, subsequent discrete shed vortices were assumed to leave the trailing edge with a strength sufficient to satisfy the normal velocity requirement at the control point. The increment in circulation computed for each discrete trailing vortex was then added to the bound vortex strength.

The results of the two-dimensional wing computation were compared to Jones' exponential approximation, and the maximum deviation in bound vortex strength, throughout the transient build-up, was found to be only about 3 percent.

Having verified the computational approach for a two-dimensional wing, the method was extended to finite wings, using 20 vortex elements and control points across the span. A series of computations was made for

untapered wings of aspect ratio 6 for sweep angles up to 30 degrees. The computed time histories were then used to fit exponential approximations of the form:

$$C_{L\alpha} = K_1(1 - K_2 \text{EXP}(-K_3 S)) \quad (92)$$

where S is the distance traveled in half-chord lengths.

With this form of the approximation, K_1 is completely determined by the final steady-state value, K_2 is completely determined by the ratio of initial to final values, and K_3 depends on the rise time. To fit equation (92), the value of $C_{L\alpha}$ AT $S = 2.5$ was chosen for the determination of K_3 .

Table IX lists the results of the computations.

In the transfer function used in the equation of motion, the constants which appear are related to K_1 , K_3 , and the ratio of final to initial values of $C_{L\alpha}$. It is important to note that the ratio of final to initial values changes very little over the range of sweep angles used, and the small variation in K_3 appears to be computational "noise".

From these results, it was concluded that the only adjustment needed for swept wing indicial response is an adjustment of the steady-state lift curve slope (K_1) as a function of sweep angle. The remaining constants are embedded in equation (42) of appendix A and were unchanged for variations in sweep angle.

To estimate the noncirculatory transient lift forces and the apparent camber due to pitching, the approach consisted of a strip integration, across the span, of the two-dimensional unsteady lift and moment equations given as equations 5-311 and 5-312 of reference 11. If the two-dimensional steady-state lift-curve slope of 2π used for circulatory lift in these equations is replaced by the appropriate finite-wing lift-curve slope, the integrated expressions compare very closely with the equations used in references 2, 3, and 8 for the case of zero sweep. For exact agreement, it is only necessary to replace Theodorsen's function by our aforementioned transfer-function approximation, set Jones' ratio of semiperimeter to span (E) equal to $4/\pi$, and adjust the effective angle-of-attack increment caused by pitching to be a function of hinge axis location, which required a minor change in the constant C36 (equation (43) of appendix A).

For swept wings, an additional term appears in the circulatory moment due to pitching. This is a pure moment: it is independent of hinge axis location, and does not appear anywhere as a lift force. The additional term is introduced by the constant C560, as given by equation (65) in appendix A. Strictly speaking, this coefficient should include the circulatory lift transfer function in place of the steady-state lift-curve slope, but this refinement would have added considerable complexity to equation (57) of appendix A and was not felt to be warranted for the purpose at hand.

TABLE IX. RESULTS OF INDICIAL RESPONSE
COMPUTATIONS

UNTAPERED WINGS, ASPECT RATIO 6

Sweep Angle	Final $C_{L\alpha}$	Initial $C_{L\alpha}$	Ratio Final/Initial	$C_{L\alpha}$			
				S = 2.5	K_1	K_2	K_3
0 deg	4.27	2.78	1.54	3.66	4.27	3.49	.360
10 deg	4.23	2.75	1.54	3.63	4.23	3.50	.360
15 deg	4.17	2.71	1.54	3.58	4.18	3.52	.361
20 deg	4.11	2.65	1.55	3.52	4.11	3.55	.361
25 deg	4.02	2.58	1.56	3.43	4.01	3.58	.357
30 deg	3.88	2.49	1.56	3.32	3.88	3.60	.368

APPENDIX C. AERODYNAMIC AND MASS PARAMETERS

Symbols

b	wing span, meters (feet)
\bar{c}	mean aerodynamic chord of wing, meters (feet)
$C_{L_c}, C_{L_F}, C_{L_W}$	lift coefficients of trimmer, fuselage assembly, and wing, respectively.
$C_{L\alpha_c}, C_{L\alpha_F}, C_{L\alpha_W}$	lift curve slopes of trimmer, fuselage assembly, and wing, respectively, per radian
C_ℓ	rolling moment coefficient
$C_{\ell p}$	$\partial C_\ell / \partial \left(\frac{pb}{2U_o} \right)$, per radian
$C_{\ell r}$	$\partial C_\ell / \partial \left(\frac{rb}{2U_o} \right)$, per radian
$C_{\ell \beta}$	$\partial C_\ell / \partial \beta$, per radian
$C_{\ell \delta_c}$	$\partial C_\ell / \partial \delta_{c_r}$, per radian
$C_{\ell \delta_{t_r}}$	$\partial C_\ell / \partial \delta_{t_r}$, per radian
C_m	pitching moment coefficient of fuselage assembly
$C_{m\alpha_f}$	$\partial C_m / \partial \alpha_f$, per radian
C_{mq}	$\partial C_m / \partial \left(\frac{q\bar{c}}{2U_o} \right)$, per radian
C_{mR}	pitching moment coefficient of right trimmer
C_{mRp}	$\partial C_{mR} / \partial \left(\frac{pb}{2U_o} \right)$, per radian
C_{mRr}	$\partial C_{mR} / \partial \left(\frac{rb}{2U_o} \right)$, per radian
$C_{mR\delta}$	$\partial C_{mR} / \partial \delta_c$, per radian

$C_{mR\dot{\delta}_c}$	$\partial C_{mR} / \partial \left(\frac{\dot{\delta}_c}{2U_o} \right)$, per radian
$C_{mR\delta_t}$	$\partial C_{mR} / \partial \delta_{t_r}$, per radian
$C_{mR\beta}$	$\partial C_{mR} / \partial \beta$, per radian
C_n	yawing moment coefficient
C_{np}	$\partial C_n / \partial \left(\frac{pb}{2U_o} \right)$, per radian
C_{nr}	$\partial C_n / \partial \left(\frac{rb}{2U_o} \right)$, per radian
$C_{n\beta}$	$\partial C_n / \partial \beta$, per radian
$C_{n\delta_c}$	$\partial C_n / \partial \delta_{c_r}$, per radian
$C_{n\delta_{t_r}}$	$\partial C_n / \partial \delta_{t_r}$, per radian
C_y	side force coefficient
C_{yp}	$\partial C_y / \partial \left(\frac{pb}{2U_o} \right)$, per radian
C_{yr}	$\partial C_y / \partial \left(\frac{rb}{2U_o} \right)$, per radian
$C_{y\beta}$	$\partial C_y / \partial \beta$, per radian
g	acceleration of gravity, meters/second ² (feet/second ²)
$I_{xxT}, I_{zzT}, I_{xzT}$	moments and product of inertia of total airplane in stability axis system, kilogram-meters ² (slug-feet ²)
I_{xy_z}, I_{yz_c}	products of inertia of trimmer, kilogram-meters ² (slug-feet ²)
I_{yf}	pitching moment of inertia of fuselage assembly about hinge axis, kilogram-meters ² (slug-feet ²)

I_y' , I_y''	pitching moments of inertia of wing and trimmer, respectively, about their hinge axis, kilogram-meters ² (slug-feet ²)
l_{vt}	distance of vertical tail center of pressure aft of center of gravity, meters (feet)
m	total of mass of aircraft
m_c , m_f , m_{wb}	mass of each trimmer, fuselage assembly, and wing/boom assembly, respectively, kilograms (slugs)
α_F	angle of attack of fuselage assembly, radians
β	sideslip angle, positive wind from right, radians
δ_c	trimmer angular displacement with respect to wing, positive trailing-edge down, radians
δ_{c_r}	right trimmer displacement, radians
δ_{t_r}	displacement of trim tab on right trimmer, positive trailing-edge down, radians

Longitudinal Parameters

Lift-curve slope. The lift-curve slopes for the isolated wing and trimmer surfaces were obtained from a vortex lattice program using 15 spanwise vortex elements per semispan. For the tip-mounted aft trimmers, each trimmer was represented as a rectangular surface of aspect ratio 3. In all other computations, an aspect ratio of 6 was assumed. The values are listed in table X.

TABLE X. LIFT CURVE SLOPES

Configuration	$C_{L\alpha_w}$	$C_{L\alpha_c}$
Straight Wing	4.343	--
10° Swept Wing	4.295	--
20° Swept Wing	4.148	--
Forward Trimmers	--	4.343
Aft Trimmers	--	3.223

Mutual interference coefficients. Because of their close proximity, the wing and trimmer have significant mutual interference effects. To account for this phenomenon, the effective induced angle of attack on each surface was computed as a function of the lift coefficient on the other surface.

Using the appropriate relative geometry of the surfaces, the influence coefficients were computed from:

$$\frac{d\alpha_c}{dC_{LW}} = \frac{C_{Lc} - C'_{Lc}}{C'_{L\alpha_c}} \frac{1}{C_{LW}} \quad (93)$$

$$\frac{d\alpha_W}{dC_{Lc}} = \frac{C_{LW} - C'_{LW}}{C'_{L\alpha_W}} \frac{1}{C_{Lc}}$$

In equations (93), the prime superscript denotes the values obtained without the presence of the other lifting surface.

The values so obtained are given in table XI.

TABLE XI. MUTUAL INTERFERENCE COEFFICIENTS

Configuration	$\frac{d\alpha_c}{dC_{LW}}$	$\frac{d\alpha_W}{dC_{Lc}}$
Straight Wing, 0.5 \bar{c} Fwd. Trimmer	0.1454	-0.0166
Straight Wing, 0.75 \bar{c} Fwd. Trimmer	0.0876	-0.0112
Straight Wing, 1.00 \bar{c} Fwd. Trimmer	0.0581	-0.00820
10° Swept Wing, 1.00 \bar{c} Fwd. Trimmer	0.0647	-0.0088
20° Swept Wing, 1.00 \bar{c} Fwd. Trimmer	0.0241	-0.00744
Straight Wing, Aft Tip Trimmer	0.109	0.00611
10° Swept Wing, Aft Tip Trimmer	0.118	0.00850
20° Swept Wing, Aft Tip Trimmer	0.141	0.0155

Drag coefficients. For the wing and trimmer surfaces, the profile drag coefficient was assumed to be 0.01, while the induced drag factor,

$\frac{dC_D}{dC_L^2}$, was estimated as 0.0624 in all cases.

The fuselage drag coefficient, based on wing area, was estimated to be 0.03.

Fuselage-tail lift-curve slope. The aerodynamic derivatives of the fuselage and fuselage-mounted horizontal stabilizers were estimated by assuming an equivalent circular body with area distribution as used in the aircraft shown in figure 2 of the main body of the report.

Following the method of reference 12, the lift and moment contribution of the fuselage and horizontal tail were determined. The reference point for the moment coefficients was the wing hinge axis.

The lift coefficient of the fuselage-tail assembly, as a function of fuselage angle of attack, is estimated to be:

$$C_{L_F} = 0.00751(\alpha_F - 4^\circ) + 0.000033(\alpha_F - 4^\circ)^2 + (0.0104) (0.55\alpha_F) \quad (94)$$

From this, $C_{L_{\alpha_F}} = 0.758$ per radian.

Fuselage static angle of attack stability. The slope of the fuselage moment coefficient with respect to angle of attack is

$$C_{m_{\alpha_F}} = -0.006 - 0.00015\alpha_F \text{ per degree} \quad (95)$$

From this, $C_{m_{\alpha_F}} = -0.344$ per radian. (96)

Pitch damping coefficient. The pitch damping coefficient was estimated by assuming that all damping arises from the forces on the horizontal tail. On this basis, $C_{m_q} = -4.76$ per radian.

Longitudinal mass parameters. The mass and pitching inertia parameters for the fuselage-tail assembly were constant for all configurations. The pitching moment of inertia, I_{y_F} , was 1232.34 kilogram-meter² (908.87 slug-foot²); and the mass, m_F , was 568.61 kilograms (38.96 slugs).

The corresponding parameters for the wing/boom/trimmer assembly are configuration dependent and are listed in table XII.

TABLE XII. LONGITUDINAL MASS PARAMETERS FOR WING/
TRIMMER ASSEMBLY

Configuration	I_y'	I_y''	m_c	m_{wb}
Straight Wing, 0.5 \bar{c} Fwd Trimmer	34.06 (25.12)	0.9586 (0.707)	27.73 (1.90)	141.13 (9.67)
Straight Wing, 0.75 \bar{c} Fwd Trimmer	36.92 (27.23)	0.6522 (0.481)	21.45 (1.47)	125.23 (8.58)
Straight Wing, 1.00 \bar{c} Fwd Trimmer	36.20 (26.70)	0.4827 (0.356)	17.51 (1.20)	122.45 (8.39)
10° Swept Wing, 1.00 \bar{c} Fwd Trimmer	55.12 (40.65)	0.4827 (0.345)	17.51 (1.20)	126.38 (8.66)
20° Swept Wing, 1.00 \bar{c} Fwd Trimmer	81.32 (59.97)	0.4827 (0.356)	17.51 (1.20)	134.71 (9.23)
Straight Wing, Aft Free Trimmer	130.5 (96.27)	1.46 (1.08)	36.78 (2.52)	204.91 (14.04)
10° Swept Wing, Aft Free Trimmer	120.2 (88.66)	1.46 (1.08)	36.78 (2.52)	188.86 (12.94)
20° Swept Wing, Aft Free Trimmer	146.9 (108.34)	1.46 (1.08)	36.78 (2.52)	191.63 (13.13)
Straight Wing, Aft Fixed Trimmer	117.6 (86.71)	1.46 (1.08)	36.78 (2.52)	166.97 (11.44)
10° Swept Wing, Aft Fixed Trimmer	104.7 (77.19)	1.46 (1.08)	36.78 (2.52)	155.58 (10.66)
20° Swept Wing, Aft Fixed Trimmer	114.1 (84.14)	1.46 (1.08)	36.78 (2.52)	157.04 (10.76)

Lateral-Directional Parameters

Wing-trimmer contributions to lateral-directional derivatives. For the wing/trimmer assembly, a vortex lattice approach was used to compute increments in pitching, yawing, and rolling moments on the wing and trimmers for perturbations in sideslip, yawing velocity, rolling velocity, and trimmer displacement. Twenty vortex elements and associated control points were used across the span of the wing, while 10 were used on each aft trimmer surface.

Although the derivatives for rolling and yawing disturbances agree closely with reference data available in the literature for wing-only cases, the sideslip derivatives for trimmer pitching moment are open to some ques-

tion and no data are available for comparison. A more precise estimation of trimmer pitching moment response to sideslip appears to be precluded by the inability of the conventional vortex-lattice model to simulate the precise flow pattern about the wingtips in sideslip. For aft-mounted tip trimmers, the tendency of the leeward trimmer to move into the assumed wing wake raises a question of the validity of the modeling technique on that side. The assumption is made that the trailing vortices are aligned with the free-stream direction, which immerses the inboard portion of the leeward trimmer in the wake of the wingtip. This model is probably invalid in the immediate vicinity of the wingtips.

Since a more accurate model of the tip flow may be beyond the state of the art, and since no empirical data are available, a decision was made to use only the derivatives computed for the windward trimmer, where the geometry of the mathematical representation is intuitively more acceptable. Furthermore, it should be noted that the geometrical difficulty is alleviated to some extent for the swept wings because the trimmer moves forward with respect to the tip sections.

The trimmer derivatives and the wing/trimmer contribution to the total lateral-directional derivatives are listed in table XIII for the cruise condition. Separate values are given, in some cases, for the free and fixed aft trimmers. Although the geometry is similar, differences in equilibrium trimmer lift coefficient cause changes in the spanwise lift distribution, thereby affecting some of the lateral-directional derivatives.

The primary difference is in the yawing moment due to right trimmer deflection which is proverse for the free trimmer and adverse for the fixed trimmer.

Table XIV lists additional coefficients for the approach case for three values of wing sweep angle. These values apply for both the free and fixed aft trimmer cases.

Derivatives which are listed in table XIV for the straight wing, but which are not given in table XIII, apply equally well to the cruise condition.

Fuselage/tail contributions to lateral-directional derivatives.

Using the geometry of the hypothetical fuselage tail assembly, the contribution to the lateral-directional stability derivatives was first estimated in a body axis coordinate system with the x-axis aligned with the principal longitudinal axis of the assembly. The resulting values were then transformed to a stability axis system to allow for non-zero fuselage deck angles.

$C_{y\beta}$: The fuselage assembly contribution to side force with respect to sideslip angle is the sum of the fuselage and vertical tail contributions.

TABLE XIII. WING AND TRIMMER CONTRIBUTIONS TO LATERAL-DIRECTIONAL DERIVATIVES FOR CRUISE CONDITION, STRAIGHT WING

	Free Trimmer	Fixed Trimmer
$C_{m\beta}$	0.0033	-----
C_{mR_p}	-0.0266	-----
C_{mR_r}	-0.001748	-----
ΔC_{ℓ_p}	-1.031	-1.031
ΔC_{ℓ_r}	0.05385	0.1298
$C_{\ell\delta_{c_r}}$	-0.1791	-0.1788
ΔC_{n_p}	-0.04639	-0.0629
ΔC_{n_r}	-0.01542	-0.01262
$C_{n\delta_{\dot{e}}}$	-0.006224	0.004301

The procedure followed the recommended adaptation of the DATCOM (ref. 13) method outlined in reference 14. From which,

$$(C_{y\beta})_{\text{fuselage assembly}} = -0.058 \text{ per radian} \quad (97)$$

Using the procedure of reference 13 directly, the lift curve slope of the vertical tail was estimated to be 2.905 per radian. Then, using the procedure of reference 14,

$$(C_{y\beta})_{\text{vertical tail}} = -0.483 \text{ per radian} \quad (98)$$

TABLE XIV. WING AND TRIMMER CONTRIBUTIONS TO LATERAL-DIRECTIONAL DERIVATIVES FOR APPROACH CONDITION

	Wing Sweep Angle		
	0°	10°	20°
$C_{m\beta}$	0.00798	0.00696	0.00473
C_{mR_p}	-0.0266	-0.0271	-0.0284
C_{mR_r}	-0.005337	-0.00537	-0.00546
$C_{mR_{\delta_c}}$	-0.01673	-0.01703	-0.0178
ΔC_{l_p}	-1.031	-1.059	-1.131
ΔC_{l_r}	0.1057	0.1046	0.09966
ΔC_{l_β}	0.000	-0.0336	-0.0672
$C_{l_{\delta_c}}$	-0.1791	-0.1850	-0.2057
ΔC_{n_p}	-0.1057	-0.1148	-0.1206
ΔC_{n_r}	-0.03776	-0.03629	-0.03502
ΔC_{n_β}	0.000	0.017	0.019
$C_{n_{\delta_c}}$	-0.02496	-0.02514	-0.02518

Summing the two terms, the total fuselage assembly derivative, in principal body axis coordinates, is:

$$(C_{y\beta})_{\text{fuselage assembly}} = -0.541 \quad (99)$$

$C_{l\beta}$: The vertical tail is the primary fuselage assembly contributor to the rate of change of rolling moment with respect to sideslip angle. Reference 14 suggests the following equation:

$$(C_{l\beta})_{\text{vertical tail}} = -a_{VT} \frac{S_{vt}}{S} \frac{z_{vt}}{b} \eta_{vt} \quad (100)$$

Assuming that $\eta_{vt} = 1.0$,

$$(C_{l\beta})_{\text{fuselage assembly}} = -0.0569 \quad (101)$$

$C_{n\beta}$: The vertical tail is also the primary contributor to the rate of change of yawing moment with respect to sideslip. The vertical tail contribution is:

$$(C_{n\beta})_{\text{vertical tail}} = -(C_{y\beta})_{vt} \frac{l_{vt}}{b} \quad (102)$$

or,

$$(C_{n\beta})_{\text{vertical tail}} = 0.1818 \quad (103)$$

Using the procedure outlined in reference 14, the wing-fuselage interference term was estimated to be $-0.060/\text{radian}$. Summing the two terms,

$$(C_{n\beta})_{\text{fuselage assembly}} = 0.122 \quad (104)$$

C_{yp} : Examining the relationships prescribed in reference 14, it was concluded that, to good approximation, the rate of change of side force with respect to rolling rate is zero.

C_{lp} : Both the horizontal and vertical tail surfaces contribute to the rate of change of rolling moment with respect to rolling rate. Using the methods of reference 14,

$$(C_{lp})_{\text{fuselage assembly}} = -0.01088 \quad (105)$$

C_{np} : The vertical tail is assumed to be the sole contributor to the change in yawing moment with respect to rolling rate. Following reference 13,

$$(C_{np})_{\text{fuselage assembly}} = 0.042 \quad (106)$$

C_{yr} : From reference 14, a good approximation to the rate of change of side force coefficient with respect to yawing rate is:

$$(C_{yr})_{\text{fuselage assembly}} = 2(C_{n\beta})_{vt} \quad (107)$$

so,

$$(C_{yr})_{\text{fuselage assembly}} = 0.3636 \quad (108)$$

C_{ℓ_r} : Reference 13 suggests using the following expression for the rate of change of rolling moment with respect to yawing rate:

$$(C_{\ell_r})_{\text{fuselage assembly}} = -2 \frac{\ell_{vt}}{b} (C_{\ell\beta})_{vt} \quad (109)$$

so,

$$(C_{\ell_r})_{\text{fuselage assembly}} = 0.04282 \quad (110)$$

C_{nr} : For the rate of change of yawing moment with respect to yawing rate, reference 13 suggests:

$$(C_{nr})_{\text{fuselage assembly}} = 2 \left(\frac{\ell_{vt}}{b} \right)^2 (C_{y\beta})_{vt} \quad (111)$$

or,

$$(C_{nr})_{\text{fuselage assembly}} = -0.1369 \quad (112)$$

The transformation from body axes to stability axes, when the longitudinal axis of the fuselage assembly is inclined through the deck angle ϵ , is per-

formed with the following equations:

$$C_{y\beta} = C_{y\beta_B} \quad (113)$$

$$C_{y_p} = C_{y_{r_B}} \sin \epsilon \quad (114)$$

$$C_{y_r} = C_{y_{r_B}} \cos \epsilon \quad (115)$$

$$C_{l\beta} = C_{l\beta_B} \cos \epsilon + C_{n\beta_B} \sin \epsilon \quad (116)$$

$$C_{n\beta} = C_{l\beta_B} \sin \epsilon + C_{n\beta_B} \cos \epsilon \quad (117)$$

$$C_{l_p} = C_{l_{p_B}} \cos^2 \epsilon + (C_{l_{r_B}} + C_{n_{p_B}}) \sin \epsilon \cos \epsilon + C_{n_{r_B}} \sin^2 \epsilon \quad (118)$$

$$C_{l_r} = C_{l_{r_B}} \cos^2 \epsilon + (C_{n_{r_B}} - C_{l_{p_B}}) \sin \epsilon \cos \epsilon - C_{n_{p_B}} \sin^2 \epsilon \quad (119)$$

$$C_{n_p} = C_{n_{p_B}} \cos^2 \epsilon + (C_{n_{r_B}} - C_{l_{p_B}}) \sin \epsilon \cos \epsilon - C_{l_{r_B}} \sin^2 \epsilon \quad (120)$$

$$C_{n_r} = C_{n_{r_B}} \cos^2 \epsilon + (C_{l_{r_B}} - C_{n_{p_B}}) \sin \epsilon \cos \epsilon + C_{l_{p_B}} \sin^2 \epsilon \quad (121)$$

Table XV lists the fuselage assembly contributions to the lateral directional derivatives for three values of deck angle.

The total lateral-directional derivatives, for a selected combination of flight condition, deck angle, and wing/trimmer planform, are obtained by summing the contributions in tables XV and either XIII or XIV.

Lateral-directional mass parameters. The moments of inertia of the aircraft were computed about the x and z principal body axes and then transformed to stability axes. Table XVI lists the moments and products of inertia about the stability axis system.

TABLE XV. FUSELAGE ASSEMBLY CONTRIBUTIONS TO LATERAL-DIRECTIONAL DERIVATIVES

	Deck Angle		
	15°	0°	+15°
$\Delta C_{y\beta}$	-0.541	-0.541	-0.541
ΔC_{yp}	-0.0941	0.	0.0941
ΔC_{yr}	0.3412	0.3636	0.3512
$\Delta C_{\ell\beta}$	-0.0865	-0.0569	-0.0234
$\Delta C_{\ell p}$	-0.03904	-0.00928	0.003381
$\Delta C_{\ell r}$	0.06906	0.04284	0.005252
$\Delta C_{n\beta}$	0.1031	0.1220	0.1326
ΔC_{np}	0.0682	0.0420	0.004412
ΔC_{nr}	-0.1071	-0.1369	-0.1496

TABLE XVI. MOMENTS AND PRODUCTS OF INERTIA

Fuselage Deck Angle	I_{xx_T}		I_{zz_T}		I_{xz_T}	
-15°	1300.8	(959.35)	2006.0	(1479.4)	205.98	(151.91)
0	1245.6	(918.65)	2061.2	(1520.1)	0.	
+15°	1300.8	(959.35)	2006.0	(1479.4)	-204.98	(-151.91)

The products of inertia for the trimmer surfaces, I_{xy_c} and I_{yz_c} , were zero in all cases.

APPENDIX D. METHOD OF COMPUTING TURBULENCE RESPONSES

Symbols

b	wing span, meters (feet)
L	scale length of turbulence, meters (feet)
U_0	airspeed, meters/second (feet/second)
σ_x	rms value of variable x
Φ	power spectral density function
Ω	spatial frequency, radians/meter (radians/foot)

Longitudinal Responses

Equation (1) in this report describes the deterministic response of the longitudinal system to the vertical gust velocity.

For random turbulence responses, the frequency response function is used to compute the spectrum of the response for each variable of interest. The output spectrum for a variable, x, is given by the following equation (reference 15):

$$\sigma_x(\Omega) = \left| \frac{x}{V_g} \right|^2 \Phi(\Omega) \quad (122)$$

where $\frac{x}{V_g}$ is the modulus of a frequency response function which defines the response of the variable to the gust velocity.

The root-mean-square response of the variable is the quantity of interest, and it is then computed from:

$$\sigma_x = \left[\int_0^{\infty} \Phi_x(\Omega) d\Omega \right]^{1/2} \quad (123)$$

The frequency response function was computed directly at each frequency. In complex notation, a unit sinusoidal gust velocity was represented as $j\omega$ in the equations of motion. Solving the complex set of equations, the steady-state response of each variable of interest was computed for each value of the sinusoidal gust velocity frequency, ω . The absolute magnitude of the response function was then computed at each frequency to obtain the desired frequency response function for equation (122).

In the numerical integration of equation (123), the actual limits of integration were from spatial frequencies corresponding to temporal

frequencies ranging from 0.3 to 40 radians per second, using the relationship

$$\Omega = \frac{\omega}{U_0} \quad (124)$$

Only vertical gust components were considered, and the Dryden power spectral density function was used with a scale length of 533.4 meters (1750 feet) and an rms gust intensity of 0.305 meter per second (1 foot per second). The Dryden spectrum is given by

$$\Phi(\Omega) = 0.0283 \sigma_g^2 \frac{L}{\pi} \frac{1 + 3\Omega^2 L^2}{(1 + \Omega^2 L^2)^2} \quad (125)$$

Lateral-Directional Responses

Equation (2) of the main body of the report describes the deterministic response of the system to rolling and sideslip gusts. Two forcing functions are present in equation (2), and these functions are uncorrelated in the statistical sense.

Since the turbulence is assumed to be homogeneous isotropic, the vertical and side gust components measured at the same point on the airplane have the same spectrum, and both components have the same rms value. The sideslip gust is directly related to the side gust velocity, but the rolling gust is based upon the spanwise gradient of the vertical gust velocity.

Because the side and vertical gust components are uncorrelated, the total response of the aircraft, in a variable x , is computed from

$$\Phi_x(\Omega) = \left| \frac{x}{\dot{\phi}_g} \right|^2 \Phi_{\dot{\phi}_g}(\Omega) + \left| \frac{x}{\beta_g} \right|^2 \Phi_{\beta_g}(\Omega) \quad (126)$$

where $\left| \frac{x}{\dot{\phi}_g} \right|$ and $\left| \frac{x}{\beta_g} \right|$ are the moduli of frequency-response functions for the response of the variable x to the rolling and sideslip gusts, respectively. The spectrum of the sideslip gust is simply related to the spectrum given in equation (125) and is, for unit gust intensity,

$$\Phi_{\beta_g} = \frac{L}{\pi U_0^2} \frac{1 + 3\Omega^2 L^2}{\left[1 + \Omega^2 L^2 \right]^2} \quad (127)$$

The power spectrum of the rolling gust was obtained from reference 15, wherein a quantity, ϕ_2 , is derived which is equivalent to one-half the rolling gust power spectral density function used in equation (126). This rolling-gust spectrum is, for unit intensity,

$$\begin{aligned} \Phi_{\phi_g}(\Omega) &= \frac{1}{\pi L} \left(\frac{L^2 \Omega^2}{1 + L^2 \Omega^2} \right) g^3 \\ &+ \frac{3}{2} \frac{1}{\pi L} \left[\ln \left(\frac{1-g}{1+g} \right) - 2g - \frac{2}{3} g^3 \right] \end{aligned} \quad (128)$$

where,

$$g = \frac{\pi L/b}{\sqrt{1 + L^2 \Omega^2 + (\pi L/b)^2}} \quad (129)$$

The frequency response functions needed for equation (126) were obtained numerically and the root-mean-square responses were computed from equation (123).

REFERENCES

1. Townsend, Lew: "Movable Wing Controls Flying Boat", The AOPA Pilot, Vol. 12, No. 9, September 1969.
2. Porter, Richard F.; and Brown, Joe H., Jr.: Evaluation of the Gust-Alleviation Characteristics and Handling Qualities of a Free-Wing Aircraft. NASA CR-1523, July 1970.
3. Porter, Richard F.; Luce, Ross G.; and Brown, Joe H., Jr.: Investigation of the Applicability of the Free-Wing Principle to Light General Aviation Aircraft. NASA CR-2046, June 1972.
4. Ormiston, Robert A.: Experimental Investigation of Stability and Stall Flutter of a Free-Floating Wing V/STOL Model. NASA TN D-6831, June 1972.
5. Moran, W. J.: Control Surface Sizing Model for the Torsionally Free Wing. General Dynamics, Fort Worth Div., ERR-FW-1555, December 31, 1973.
6. Rankin, E. E.: Torsionally Free Wing Subscale Remotely Piloted Research Vehicle Design and Flight Test. General Dynamics, Fort Worth Div., ERR-FW-1490, December 1973.
7. Gee, Shu W.; and Brown, Samuel R.: Flight Tests of a Radio-Controlled Airplane Model with a Free-Wing, Free-Canard Configuration. NASA TM-72853, March 1978.
8. Porter, Richard F.; Hall, David W.; Brown, Joe H., Jr.; and Gregorek, Gerald M.: Analytical Study of a Free-Wing/Free-Trimmed Concept. NASA CR-2946, February 1978.
9. Chalk, C. R.; Neal, T. P.; Harris, T. M.; Pritchard, F. E.; and Woodcock, R. J.: Background Information and User Guide for MIL-F-8785B(ASG), "Military Specification-Flying Qualities of Piloted Airplanes" AFFDL-TR-69-72, Air Force Flight Dynamics Lab., Wright-Patterson Air Force Base, August 1969.
10. Jones, Robert T.: The Unsteady Lift of a Wing of Finite Aspect Ratio. NACA TR 681, 1941.
11. Bisplinghoff, Raymond L.; Ashley, Holt; and Halfman, Robert L.: Aeroelasticity. Addison-Wesley Publishing Company, Inc., Cambridge, Mass., 1955.
12. Wolowicz, Chester H.; and Yancey, Roxannah B.: Longitudinal Aerodynamic Characteristics of Light, Twin-Engine, Propeller-Driven Airplanes. NASA TN D-6800, 1972.
13. Hoak, D. E., et al.: USAF Stability and Control DATCOM, USAF/ASD, Air Force Flight Dynamics Lab., Wright-Patterson Air Force Base, October 1960.

14. Smetana, Frederick O.; et al: Riding and Handling Qualities of Light Aircraft - A Review and Analysis. NASA CR-1975, March 1972.
15. Etkin, B.: A Theory of the Response of Airplanes to Random Atmospheric Turbulence. Aero/Space Sciences, July 1959, pp. 409-420.

1. Report No. NASA CR-3135	2. Government Accession No.	3. Recipient's Catalog No.	
4. Title and Subtitle EXTENDED ANALYTICAL STUDY OF THE FREE-WING/ FREE-TRIMMER CONCEPT		5. Report Date April 1979	6. Performing Organization Code
		8. Performing Organization Report No.	
7. Author(s) Richard F. Porter, David W. Hall, and Rodolfo D. Vergara		10. Work Unit No.	
9. Performing Organization Name and Address Battelle Columbus Laboratories 505 King Avenue Columbus, Ohio 43201		11. Contract or Grant No. NASA-2498	
		13. Type of Report and Period Covered Contractor Report - Final	
12. Sponsoring Agency Name and Address National Aeronautics and Space Administration Washington, D. C. 20546		14. Sponsoring Agency Code H-1067	
		15. Supplementary Notes NASA Technical Monitor: Shu W. Gee, Dryden Flight Research Center	
16. Abstract <p>This report describes an extension of the analytical study of the free-wing/free-trimmer concept which was documented in NASA Contractor Report 2946 to: (1) compare the fore and aft trimmer configurations on the basis of equal lift capability, rather than equal area; (2) assess the influence of tip-mounted aft trimmers, both free and fixed, on the lateral-directional modes and turbulence responses; (3) examine the feasibility of using differential tip-mounted trimmer deflection for lateral control; (4) determine the effects of independent fuselage attitude (deck angle) on the lateral-directional behavior; and (5) estimate the influence of wing sweep on dynamic behavior and structural weight.</p> <p>The forward trimmer concept is feasible with the reduced size examined in this study, but it remains inferior to the aft trimmer arrangement in every respect except structural weight. The tip-mounted aft free-trimmer has excellent vertical gust alleviation and good control response behavior.</p> <p>If the aft trimmer is not free, the weight penalty is reduced and the trimmed lift capability can be increased substantially for the same wing/trimmer geometry.</p> <p>Differential motion of the aft trimmer is found to provide powerful lateral control; while the effect of fuselage deck angle is a reduction of the dutch roll damping ratio for nose-down attitudes.</p>			
17. Key Words (Suggested by Author(s)) Free wing Aerodynamics Aircraft design		18. Distribution Statement Unclassified - Unlimited STAR category: 02	
19. Security Classif. (of this report) Unclassified	20. Security Classif. (of this page) Unclassified	21. No. of Pages 94	22. Price* \$4.75

*For sale by the National Technical Information Service, Springfield, Virginia 22161